Synthesis of minerals

Iskrina A.V.[1], Spivak A.V.[1], Setkova T.V.[1], Khasanov S.S.[2], Kuzmin A.V.[2], Zakharchenko E.S.[1], Viryus A.A.[1] **Synthesis and structural characteristics of a new compound $GaGeO_3OH$ - an analogue of the Egg phase $AlSiO_3OH$.**

[1] D.S. Korzhinskii Institute of Experimental Mineralogy of RAS, Chernogolovka, spivak@iem.ac.ru

[2] Osipyan Institute of Solid State Physics of Russian Academy of Sciences, Chernogolovka,

Abstract. We present a complex study (scanning electron microscopy, energy dispersive X-ray spectroscopy, powder X-ray diffraction, and Raman spectroscopy) on the synthetic GaGeO3OH compound. For the first time, the $GaGeO_3OH$ crystals (up to 10 μm in size) are synthesized at 7GPa and 1000 °C. The unit cell parameters are: a = 7.5785(1) Å, b = 4.4605(3) Å, c = 7.2469(4) Å, β = 97.519(2)°, V = 242.87(02) Å^3, space group is $P2_1/n$; and are characterized by large values compared to the natural and synthetic Egg phase. The experimentally obtained Raman spectrum of $GaGeO_3OH$ has a topology similar to the Raman spectra of the Egg phase (natural and synthetic $AlSiO_3OH$ and model $MgSiO_4H_2$). In the high-frequency region of the Raman spectra, a group of wide OH^- vibration bands is recorded, which indicates the presence of several hydrogen positions in the crystal structure of $GaGeO_3OH$.

Keywords: *phase Egg, synthesis, gallium, germanium, crystal structure*

Introduction. One of the relevant areas of experimental mineralogy, petrology, and geochemistry is the study of high-pressure phases of possible H_2O reservoirs in the mantle transition zone. Within the framework of the Al_2O_3 – SiO_2 – H_2O model system, most of the research has focused on studying the Egg phase, first described by Eggleton et al. (1978). Later, this phase was discovered in inclusions in ultra-deep diamonds (Wirth et al., 2007). The crystal structure of $AlSiO_3OH$, including the position of hydrogen, was solved and refined using high-resolution X-ray powder diffraction: a = 7.14409(2) Å, b = 4.33462(1) Å, c = 6.95253(2) Å and β = 98.396(1) Å, Z = 4, V_0 = 212.99(1) Å^3, space group is $P2_1/n$ (Schmidt et al., 1998). The model end member of the $MgSiO_4H_2$ solid solution ($P2_1/n$) with $AlSiO_3OH$, according to the substitution of $Al^{3+} \leftrightarrow Mg^{2+} + H^+$, was synthesized at 24 GPa and 1400 °C (Bindi et al., 2020). This paper presents the results of the synthesis of a new compound $GaGeO_3OH$, an analog of the Egg phase $AlSiO_3OH$, as well as data on the refinement of its crystal structure.

Methods. The synthesis experiments were carried out using a toroidal anvil apparatus at the D.S. Korzhinsky Institute of Experimental Mineralogy of the Russian Academy of Sciences (IEM RAS). The toroidal anvil apparatus is a modification of the Bridgman anvil apparatus (Litvin, 1991). A powdered mixture of gallium (99.5%) and germanium (99.9%) oxides was used as the starting material. The oxides were mixed in a 1:1 ratio and placed in a Pt ampoule with the addition of excess deionized water. The experiment was carried out at P=7.0 GPa and T=1000°C for 6 hours. The pressure was determined using the standard Bi polymorphisms (at 2.55, 2.7, and 7.7 GPa), Tl (at 3.67 GPa), and Ba (5.5 GPa) with an accuracy of 0.25 GPa. The temperature was controlled and measured by a thermocouple ($Pt_{70}Rh_{30}/Pt_{94}Rh_6$) with an accuracy of ± 20°C. After the experiment, the sample was cooled to 20°C at a rate of 300 ± 50°C/s.

The morphology of the obtained crystals and composition were studied using a Tescan Vega II XMU scanning electron microscope (SEM) using secondary and reflected electron detectors, as well as an energy-dispersive X-ray spectrometer (INCAx-sight) for quantitative analysis. Electron microprobe analysis (EMPA) of the studied samples was performed at an accelerating voltage of 20 kV, an absorbed electron current of 0.2 nA, and a probe size of 0.3 μm. The analysis time was 70 s. The following standards were used for the quantitative determination of the main elements: for Ge – elemental germanium, for Ga – GaP.

The Raman spectra of the crystals were measured on a setup consisting of an Acton SpectraPro-2500i spectrograph with a Pixis2K CCD detector cooled to -70°C and an Olympus microscope with a continuous solid-state monomeric laser with a wavelength of 532 nm. The laser beam was focused on the sample using an Olympus 50× lens into a spot with a diameter of ~5 μm. Raman data were collected by repeated exposures of 540 s (3 × 180 s). The software Fityk 1.3.1 was used for profile fitting for the Raman band analysis.

Powder X-ray diffraction data were collected with BRUKER D8Advance using capillary scheme at ambient conditions (atmospheric pressure, 25˚C). The 0.30 mm capillary was loosely filled with a fine powder of the synthesized phase. Johanson monochromator with $CuK\alpha_1$ radiation and with focus on the detector was used for the primary beam. In addition to sharp diffraction peaks, the spectrum contained a broad diffuse maximum resulting from scattering at the amorphous capillary material. To better approximate the background of the spectrum, this diffuse maximum was subsequently considered as a contribution from the amorphous minor phase.

The resulting peak profiles and the refinement of the peak positions and all spectra, the determination

of the lattice parameters and the related indexing of the observed diffraction maxima were carried out according to the standard procedures of the TOPAS software Ver. 4.2 (Bruker AXS, Topas V4, 2008). Special attention was paid to the accuracy of the refinement of the spectral background, since many weak reflections were observed. The obtained values of the lattice parameters and the characteristics of the diffraction spectrum were used in the solution of the structure. It should be noted that the indexing and unit cell determination procedure was stable with different choices of the first 25–40 reflexes, with different levels of clipping of weak peaks, and with different variants of the analytical form of maxima.

To solve the structure, the method of simulated annealing was used in the mode of comparison of experimental and theoretical spectra using the advanced features of the TOPAS software package. The composition of the cell was set as 4 Ga atoms, 4 Ge atoms and 16 oxygen atoms, according to the data of elemental analysis and space filling analysis. In accordance with the symmetry group $P2_1/n$ (below), the coordinates of the independent part of the structure, $Ga1Ge1O_4$, were determined. The structure solution routine quickly comes to a stable configuration of atoms (Ga and Ge atoms in an octahedral coordination of oxygen atoms) with a confidence factor of about R_{wp} = 17 %.

The resulting structure model was further refined without constraints by using the standard method of full-profile fitting of X-ray diffraction spectra (Rietveld method) in the TOPAS software to the reliability factors R_{wp} = 4.05 %, R_p = 3.06 % and R_{exp} = 2.86 %, consequently χ^2 = 1.42, and R_{Bregg} = 1.47 %, which is a good indicator of the confidence of the final structure model.

Results and discussion. As a result of the experiments, a fine crystalline powder is formed in the entire volume of the capsule. White crystals have the isometric shape of a pseudocubic habitus. The size of individual crystals reaches 5-8 microns (Fig. 1). The chemical composition is defined as Ga_2O_3 40.9 ± 0.8, GeO_2 43.8 ± 0.8% by weight. The crystals used for X-ray diffraction are homogeneous within the limits of analytical error.

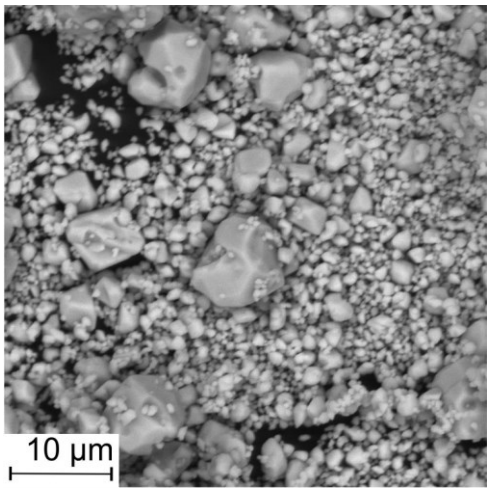

Fig. 1. SEM images of synthesized $GaGeO_3OH$ crystal**s.**

X-ray diffraction analysis revealed that the $GaGeO_3OH$ phase crystallizes in the $P2_1/n$ (14) space group with unit cell parameters: a = 7.5785(1) Å; b = 4.4605(3) Å; c = 7.2469(4) Å; V = 242.87(02) Å^3; β = 97.519(2). The structure of $GaGeO_3OH$ consists of GeO_6 octahedra connected by common edges and a Ga_2O_{10} dimer, similar to the pure Egg phase of $AlSiO_3OH$ (Schmidt et al., 1998) (Fig. 2). The connection of these elements to form the structure of the Egg phase is similar to the connection of elements of another high–pressure phase, stishovite, in which octahedra connected by edges form columns of octahedra connected by corners. Two of the longest bonds in the GaO_6 and GeO_6 octahedra, GeO_2 (1,925Å) and GeO1 (2,057Å), are connected to a tetrahedral hole in the structure. The elongation of the bonds may indicate the presence of a hydrogen atom in this hole. Perhaps the hydrogen atom is not stable, but "migrates" between oxygen atoms in this tetrahedral hole.

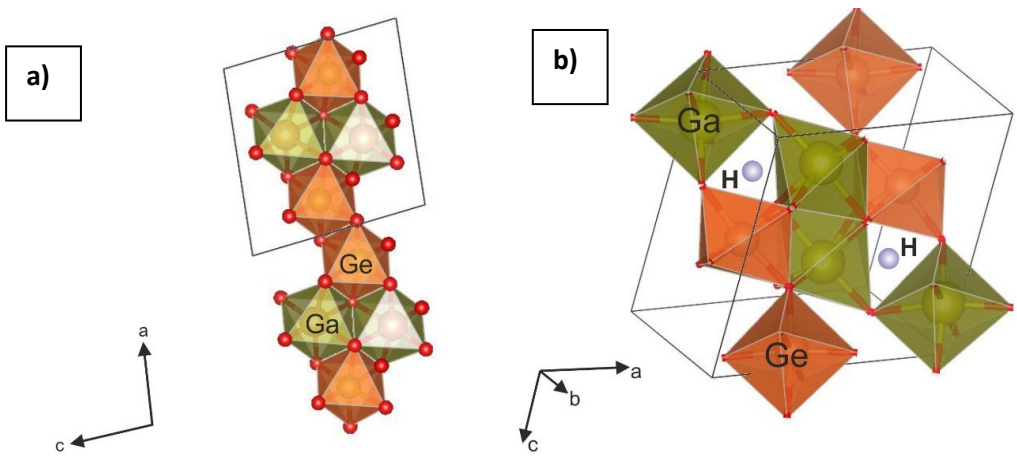

Fig. 2. Crystal structure of $GaGeO_3OH$. (a). The structural module in *a-c* projection. (b) The structure unit-cell and position of H atom in tetrahedral holes.

For the crystal structure of $GaGeO_3OH$ ($P2_1/c$), the factor group analysis predicts 18Ag + 18Bg Raman active modes. The experimental Raman spectrum for the compound $GaGeO_3OH$ was obtained in two regions of 150-1300 cm^{-1} and 2000-4000 cm^{-1} (Fig. 3). The experimentally obtained Raman spectrum has a topology similar to the Raman spectra of the Egg phase (natural and synthetic $AlSiO_3OH$ and model $MgSiO_4H_2$). Bands in the low-frequency region of the spectrum <300 cm^{-1} (~180, 190, 240, 267, 292 and 311 cm^{-1}) can be attributed to vibrational and translational vibrational modes (Michel et al., 1996; Shi et al., 2020). Bands in the region 300-950 cm^{-1} (~339, 374, 387, 428, 477,521, 603, 644, 701, 737, 826 and 912) relate to vibrational modes of GeO_6 and GaO_6 octahedra (Rudolph et al., 2002; Rao et al., 2005; Shi et al., 2020). Several wide bands of ~ 2330, 2436, 2878, 3152, and 3430 cm^{-1} are recorded in the OH-group oscillation region. Such a different position of the OH-oscillation frequencies depends on both the length of the O···O and the angle H-O-O in the environment of the O-H···O bond (Hofmeister et al., 1999). Indeed, the calculated Raman spectra of the Mg-Egg phase suggest the presence of two vibrational modes at ~2850 and ~3475 cm^{-1} corresponding to O-H bonds with different structural parameters (Solomatova et al., 2022). Thus, a group of wide bands recorded in the OH-group oscillation region indicates the presence of several positions of hydrogen in the crystal structure of $GaGeO_3OH$.

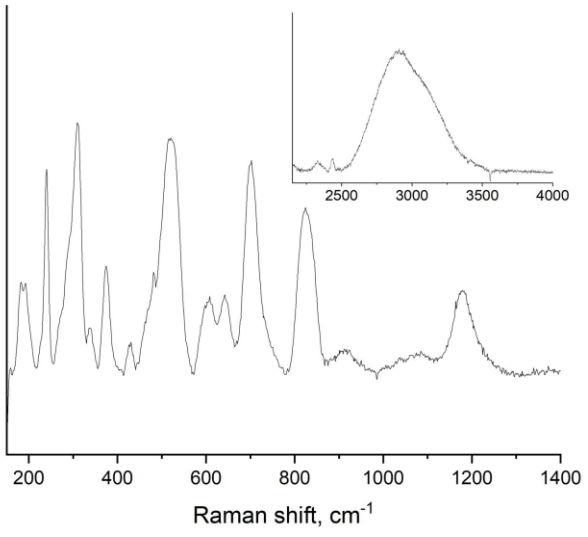

Fig. 3. The Raman spectra of the compound $GaGeO_3OH$.

Conclusions. For the first time, $GaGeO_3OH$ crystals (up to 10 μm) were synthesized at a temperature of 1000°C and a pressure of 7 GPa. The synthetic compound crystallizes in the same monoclinic structure with the space group $P2_1/n$ as the Egg phase $AlSiO_3OH$. The unit cell parameters of the synthesized $GaGeO_3OH$ phase (a = 7.5785(1)Å, b = 4.4605(3)Å, c = 7.2469(4)Å, β = 97.519(2)°, V = 242.87(02)Å^3) are characterized by higher values compared to the natural and synthetic Egg phases. The factor group analysis predicts that 36 modes are very active. The experimentally obtained Raman spectrum has a topology similar to the Raman spectra of the Egg phase (natural and synthetic $AlSiO_3OH$ and model $MgSiO_4H_2$). A group of wide OH-oscillation bands was detected in the high-frequency region of the Raman spectra, which indicates the presence of several hydrogen positions in the crystal structure of $GaGeO_3OH$. Thus, the synthetic compound $GaGeO_3OH$ can be considered as an analog of the Egg phase.

Acknowledgments

This research was financially supported by the Russian Science Foundation, grant number 24-27-00078.

References

Bindi L., Bendeliani A., Bobrov A., Matrosova E., Irifune T. Incorporation of Mg in phase Egg, $AlSiO_3OH$: Toward a new polymorph of phase H, $MgSiH_2O_4$, a carrier of water in the deep mantle // Am. Mineral. 2020. Vol. 105. P. 132–135. https://doi.org/10.2138/am-2020-7204

Bruker AXS, Topas V4: general profile and structure analysis software for powder diffraction data, - User's Manual, Bruker AXS. 2008.

Eggleton R.A., Chappell B.W. The crystal structure of stilpnomelane. Part III: Chemistry and physical properties // Mineral. Mag. 1978. V. 42. P. 361–368. https://doi.org/10.1180/minmag.1978.042.323.06

Hofmeister A.M., H. Cynn, P.C. Burnley, C. Meade, Vibrational spectra of dense, hydrous magnesium silicates at high pressure: Importance of the hydrogen bond angle// Am. Mineral. Vol. 84. 1999. 454–464. https://doi.org/10.2138/am-1999-0330

Litvin Y.A., Physico-chemical studies of the melting of the Earth's deep substance // Science. 1991. Vol. 312. Moscow.

Michel D., Colomban P., Abolhassani S., Voyron F., Kahn-Harari A. Germanium Mullite: Structure and Vibrational Spectra of Gels, Glasses and Ceramics // J. Eur. Ceram. Soc. 1996. Vol. 16. P. 161–168. https://doi.org/10.1016/0955-2219(95)00145-X

Rao R., Rao A.M., Xu B., Dong J., Sharma S., Sunkara M.K. Blueshifted Raman scattering and its correlation with the [110] growth direction in gallium oxide nanowires // J. Appl. Phys. 2005. Vol. 98. https://doi.org/10.1063/1.2128044

Schmidt M.W., Finger L.W., Angel R.J., Dinnebier R.E. Synthesis, crystal structure, and phase relations of $AlSiO_3OH$, a high-pressure hydrous phase // Am. Mineral. 1998. Vol. 83 P. 881–888. https://doi.org/10.2138/am-1998-7-820

Schulze K., Pamato M.G., Kurnosov A., Ballaran T.B., Glazyrin K., Pakhomova A., Marquardt H. High-pressure single-crystal structural analysis of

$AlSiO_3OH$ phase egg // Am. Mineral. 2018. Vol. 103. P. 1975–1980. https://doi.org/10.2138/am-2018-6562
Shi F., Qiao H. Influence of hydrothermal reaction time on crystal qualities and photoluminescence properties of β-Ga_2O_3 nanorods// J. Mater. Sci. Mater. Electron. 2020. Vol. 31. P. 20223–20231. https://doi.org/10.1007/s10854-020-04542-w
Solomatova N.V., Caracas R., Bindi L., Asimow P.D. Ab initio study of the structure and relative stability of $MgSiO_4H_2$ polymorphs at high pressures and temperatures // Am. Mineral. 2022. Vol. 107. P. 781–789. https://doi.org/10.2138/am-2021-7937
Rudolph W.W., Pye C.C., Irmer G. Study of gallium(III) nitrate hydrate and aqueous solutions: Raman spectroscopy and ab initio molecular orbital calculations of gallium(III) water clusters // J. Raman Spectrosc. 2002. Vol. 33. P. 177–190. https://doi.org/10.1002/jrs.842
Wirth R., Vollmer C., Brenker F., Matsyuk S., Kaminsky F. Inclusions of nanocrystalline hydrous aluminium silicate "Phase Egg" in superdeep diamonds from Juina (Mato Grosso State, Brazil) // Earth Planet Sci. Let. 2007. Vol. 259. P. 384–399. https://doi.org/10.1016/j.epsl.2007.04.041

Iskrina A.V., Spivak A.V., Setkova T.V., Zakharchenko E.S., Viryus A.A. Comparative analysis of stability of $GaGeO_3OH$ and $AlSiO_3OH$ at high pressure (up to 30 GPa).

D.S. Korzhinskii Institute of Experimental Mineralogy of RAS, Chernogolovka, spivak@iem.ac.ru

Abstract: Gallogermanates have attracted sufficient attention as a high-pressure model of silicates and aluminosilicates due to chemical deformation of the structure. Thus, the $GaGeO_3OH$ compound can be considered as an analog of the phase Egg ($AlSiO_3OH$), which is known as a possible H_2O reservoir in the deep Earth's interior. Using *in situ* Raman spectroscopy at high pressures, the dependence of the shift in the position of the main bands of the $GaGeO_3OH$ Raman spectrum on the pressure was established. According to the data of Raman spectroscopy up to 30 GPa, it was revealed that the $GaGeO_3OH$ undergoes the possible structural changes at 4 and 14 GPa.

***Keywords**: phase Egg, synthesis, gallium, germanium, high pressure, DAC, Raman spectroscopy*

Introduction. Germanates and gallogermanates are an important class of materials attracting great interest due to a suitable combination of structural, optical, mechanical, electromagnetic and other properties for a wide range of applications in various devices (Belokoneva, 1994; Bu et al., 1998; Zhang et al., 2012; Luo et al., 2017; Lipina et al., 2019). Moreover, it was previously shown that germanates are model analogues of silicates of deep geospheres (Ringwood et al., 1963; Ringwood, 1970; Reid et al., 1970), which was confirmed in more modern works (Finger et al., 2000; Thomas et al., 2008; Stan et al., 2017). On the other hand, gallium is a chemical analog of aluminum – their outer electron shells are identical to each other like a Si–Ge pair. This geochemical similarity of aluminum with gallium and silicon with germanium makes it possible to use the Ga_2O_3-GeO_2-H_2O system as a high–impact model of the Al_2O_3 – SiO_2 - H_2O system, in which most of the research was focused on studying the stability of the $AlSiO_3OH$ Egg phase (spatial group (gr.) $P2_1/n$), first obtained by Eggleton in 1978 (Eggleton et al., 1978). Later, it was shown that the Egg phase is stable in the PT transition zone up to 21.5 GPa at 1500 °C (Fukuyama et al., 2017). *In situ* structural analysis at high pressure of the $AlSiO_3OH$ Egg phase showed that up to 16 GPa, the *b* axis is the most compressible direction, and the *β* angle decreases (Schulze et al., 2018). *Ab initio*, a study of the structure and relative stability of $MgSiO_4H_2$ polymorphs predicted a new $MgSiO_4H_2$ phase (pr. gr. $P4_32_12$) with a stability field in the range of 0-14 GPa at 1500°C (Solomatova et al., 2022).

The purpose of this work is to study the stability of a new compound, $GaGeO_3OH$, an analog of the Egg phase $AlSiO_3OH$, under baric exposure by *in situ* Raman spectroscopy.

Synthesis. Experiments on the synthesis of $GaGeO_3OH$ were carried out using a toroidal anvil apparatus at P=7.0 GPa and T=1000°C (exposure time is 6 hours) at the D.S. Korzhinsky Institute of Experimental Mineralogy of the Russian Academy of Sciences (IEM RAS). A starting mixture of powders of gallium (99.5%) and germanium (99.9%) oxides in a 1:1 ratio was placed in a Pt ampoule with the addition of excess deionized water. The accuracy of pressure and temperature determination is ± 0.25 GPa and ±20°C, respectively (Litvin, 1991). After the experiment, the sample was quenched to 20°C at a rate of 300 ± 50°C/s.

SEM, EMPA. The composition of the obtained crystals was determined by electron-microprobe X-ray spectral analysis on a Tescan Vega II XMU scanning electron microscope using an energy-dispersive X-ray spectrometer (INCAx-sight) at an accelerating voltage of 20 kV, an absorbed electron current of 0.2 nA, and a probe size of 0.3 microns. The analysis time was 70 seconds. The following standards were used for the quantitative determination of the main elements: for Ge – Ge metal, for Ga – GaP.

X-ray diffraction analysis. X-ray diffraction analysis was performed by powder diffraction. The powder diffraction spectra were captured using a BRUKER Advance D8 instrument using a copper cathode X-ray tube and a capillary for examining small amounts of the sample. The resulting model of the structure was further refined by the Rietveld method in the TOPAS program to the confidence

factors R_{wp} of about 4% and R_{bregg} of 1.5%. The resulting structure corresponds to the well-known type $AlSiO_3OH$ (PhaseEGG).

Raman Spectroscopy at high pressures. Experiments on high-pressure Raman spectroscopy were carried out in a diamond anvil cell (DAC) at pressures up to 30 GPa. The DACs were equipped with anvils with a working surface size of 250 microns. The limiting gasket made of rhenium foil with a thickness of 200 microns was pre-pressed by about 30 microns, and then a hole with a diameter of ~ 125 microns was drilled into it. Several $GaGeO_3OH$ crystals were loaded into the resulting "chamber". NaCl was used as a pressure transfer medium. The use of NaCl is justified for pressures up to ~30 GPa (Mi, 2013). The pressure was determined by the calibrated shift of the fluorescence line of ruby R1 (a ruby sphere with a diameter of about 5 microns was placed inside the "chamber" of a cell with diamond anvils). The Raman spectra of $GaGeO_3OH$ crystals in a diamond anvil cell were captured on an installation consisting of an Acton SpectraPro-2500i spectrograph with a Pixis2K CCD detector cooled to -70 °C and an Olympus microscope with a continuous solid-state monomeric laser with a wavelength of 532 nm. The laser beam was focused on the sample using an Olympus 50× lens into a spot with a diameter of ~5 μm. The signal accumulation time was 540s (3x180s). The software Fityk 1.3.1 was used for profile fitting for the Raman band analysis.

Results and discussion. The $GaGeO_3OH$ phase crystallizes in the $P2_1/n(14)$ space group with unit cell parameters: a = 7.5785(1) Å; b = 4.4605(3) Å; c = 7.2469(4) Å; V = 242.87(02) Å^3; β = 97.519(2), while forming separate white crystals of isometric shape of pseudocubic habitus up to 5-8 microns in size (Spivak et al., 2025).

The factor group analysis for the crystal structure of $GaGeO_3OH$ ($P2_1/c$) suggests the following distribution of vibrational modes: IR active $18A_u+18B_u$ ($\Gamma_{acoustic} = A_u+2B_u$); Raman active $18A_g + 18B_g$. The experimental Raman spectrum for the $GaGeO_3OH$ compound was obtained in the range of 150-4000 cm^{-1} (Fig. 1). The assignment of the main vibrational modes was performed by comparing our data with studies of similar compounds and the general position of the bands on the Raman spectra.

Table 1. Parameters of unit cells of gallium- and germanium-containing feldspars

Feldspar	a [Å]	b [Å]	c [Å]	α [°]	β [°]	γ [°]	V [Å^3]	n
$NaAlGe_3O_8$	8.387(1)	13.292(2)	7.281(1)	94.28(1)	115.97(1)	90.66(1)	726.8(3)	58
$KAlGe_3O_8$	8.854(2)	13.842(2)	7.315(2)	90.0	115.48(1)	90.0	809.3(3)	40
$CaAl_2Ge_3O_8$	8.289(2)	12.695(2)	7.309(1)	93.43(2)	116.67(2)	93.31(1)	682.9(4)	41
$CaAlGaSi_2O_8$	8.217(1)	12.940(1)	7.121(1)	93.02(1)	115.74(1)	91.29(1)	680.2(2)	70
$BaAlGaSi_2O_8$	8.661(1)	13.105(1)	7.232(1)	90.0	114.57(1)	90.0	746.6(3)	60
$Ca_{0.6}Sr_{0.4}AlGaSi_2O_8$	8.309(1)	13.014(2)	7.170(1)	91.90(1)	116.13(1)	91.44(1)	695.1(2)	56
$Ca_{0.5}Sr_{0.5}AlGaSi_2O_8$	8.347(2)	13.015(2)	7.134(1)	91.95(1)	115.68(1)	91.09(1)	697.5(3)	49
$CaAlGaSiGeO_8$	8.233(2)	13.456(1)	7.191(1)	93.10(1)	115.18(1)	91.79(1)	718.6(3)	54
$SrAlGaSiGeO_8$	8.482(2)	13.367(2)	7.228(2)	90.0	115.11(1)	90.0	742.1(4)	37
$BaAlGaSiGeO_8$	8.746(2)	13.266(2)	7.259(2)	90.0	114.85(1)	90.0	764.3(4)	52

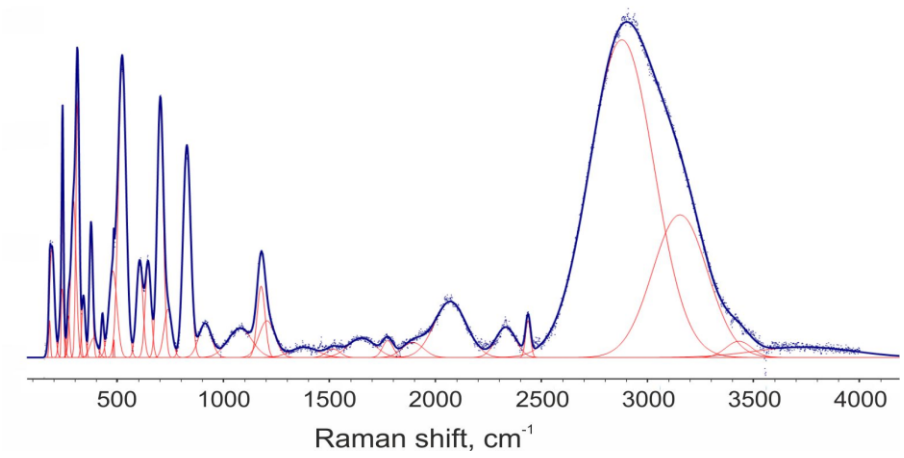

Fig. 1. The Raman spectra of the compound $GaGeO_3OH$.

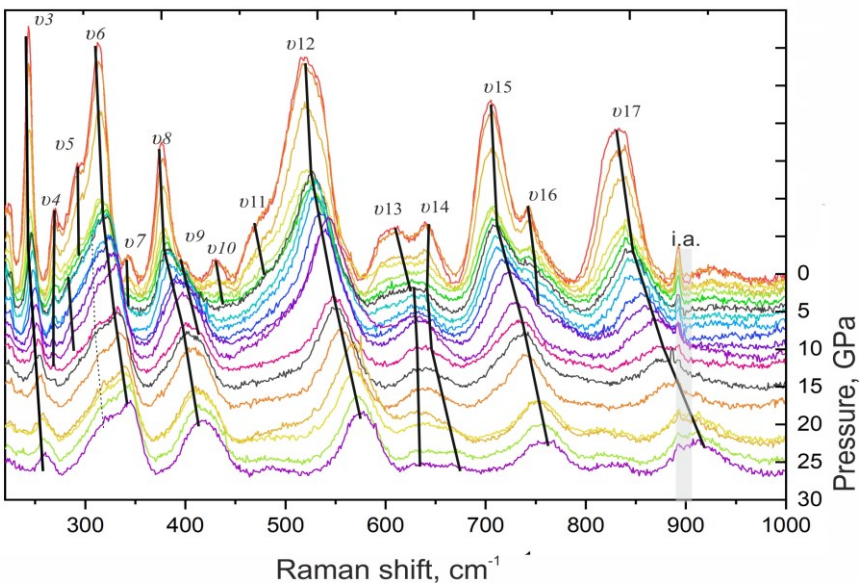

Fig. 2. Evolution of the Raman spectrum of $GaGeO_3OH$ in pressure up to ~ 30 GPa. Grey area is an instrumental artefact (i.a.) of the DAC.

A detailed study of the Raman spectra of $GaGeO_3OH$ up to ~30 GPa traced the evolution of 15 Raman bands (υ3-υ17) under compression (Fig. 2, Table 1). For bands in the region of OH-group oscillations, frequency trends could not be determined, since the intensities of these bands turned out to be relatively small during compression and decompression. In general, all the Raman bands shift to the region of higher wave numbers and become less intense with increasing pressure. As a result of processing the obtained spectroscopic data, changes in the coefficients of dependence of the frequency shifts of the Raman modes with increasing pressure were revealed. Based on this, three pressure ranges were identified depending on the value of $\partial\upsilon/\partial P$ (cm^{-1}/GPa) (Table 2). The trends in the wavenumber values for most bands in the first pressure range (from atmospheric pressure to ~ 4-5 GPa) are characterized by an insignificant value of $\partial\upsilon/\partial P$ = 0.24-1.23 cm^{-1}/GPa. At the same time, the bands of valence vibration GeO_6 (υ17 and υ13) and the band in the region of deformation vibrations and/or bending vibrations GaO_6 (υ11) have the highest value $\partial\upsilon/\partial P$ = 3,98 (0,28), 3,29 (0,18) and 3.09 (0.51) cm^{-1}/GPa, respectively. It should be noted that υ14 and υ9 have negative pressure dependence coefficients. Some less intense bands υ7, υ10, and υ11 disappear at ~ 4-5 GPa at the end of the first pressure region (Fig. 2). The coefficients of change in the wavenumber values of most bands in the second pressure region (from ~ 4-5 to ~14 GPa) have a higher value $\partial\upsilon/\partial P$ = 0.51-2.82 cm^{-1}/GPa compared to the first region. This indicates that the compression of bonds occurs more intensively in the second pressure region. The valence band GeO_6 (υ17) still has the highest value $\partial\upsilon/\partial P$ = 3.89 (0.15) cm^{-1}/GPa. The remaining "shoulder" bands υ4, υ5, υ9, and υ16 disappear at ~ 14 GPa at the end of the second pressure region (Fig. 2). The disappearance of the bands in the Raman spectrum may be due to a decrease in intensity against the general background with increasing pressure.

Table 1. The comparison of the band position of Raman spectra of $AlSiO_3OH$, $MgSiO_4H_2$ and $GaGeO_3OH$ at ambient conditions.

The assignment of the vibrational modes	υ#	**Ga,Ge-Egg** $GaGeO_3OH$ synthesized at 7 GPa/1000 °C This work	**Phase Egg** $AlSiO_3OH$ synthesized at 17 GPa/1000 °C (Xue et al., 2006)	**Phase Egg** $AlSiO_3OH$ Inclusions in diamond (Wirth et al., 2007)	**Mg-Egg** $MgSiO_4H_2$ *Ab initio* (Solomatova et al., 2022)
O-Ga-O and/or O-Ge-O libration and Ga-O and/or Ge-O translation (Shi et al., 2020; Michel et al., 1996)	υ1	179.53			
	υ 2	190.21			
	υ 3	240.09	255		
	υ 4	267.18			
	υ 5	291.76			
	υ 6	311.28			
GaO_6 deformation and bending (Shi et al., 2020; Rao et al., 2005;Rudolph	υ 7	338.82			
	υ 8	374.19	374	360	
	υ 9	386.86			

The assignment of the vibrational modes	υ#	**Ga,Ge-Egg** $GaGeO_3OH$ synthesized at 7 GPa/1000 °C This work	**Phase Egg** $AlSiO_3OH$ synthesized at 17 GPa/1000 °C (Xue et al., 2006)	**Phase Egg** $AlSiO_3OH$ Inclusions in diamond (Wirth et al., 2007)	**Mg-Egg** $MgSiO_4H_2$ *Ab initio* (Solomatova et al., 2022)
et al., 2002)	υ 10	427.95	418	419	
	υ 11	477.50	474	478	
	υ 12	521.58	521	515	
GeO_6 stretching (Okada et al., 2008; Verweij et al., 1979).	υ 13	603.33	610		
	υ 14	643.78			
	υ 15	700.64	754	757	
	υ 16	737.08			
	υ 17	826.34	898	868	
	υ 18	912.11	940		
	υ 19	1076.29			
OH bending libration (Xue et al., 2006)	υ 20	1176.77	1232		
	υ 21	1204.81			
	υ 22	2068.82	2150	2155	
OH stretching (Solomatova et al., 2022; Xue et al., 2006)	υ 23	2330.40			
	υ 24	2435.80	2450	2470	
	υ 25	2878.26	2800	2558	2850
	υ 26	3152.52		2695	
	υ 27	3430.69			3475

In the third pressure region (from ~14 to ~30 GPa), we observed eight remaining bands: υ3, υ6 in the area of vibrational O-Ga-O and/or O-Ge-O and translational Ga-O and/or Ge-O vibrations; υ8, υ12 in the area of deformation vibrations and/or bending vibrations of GaO6; υ13, υ14, υ15, υ17 in the region of valence vibrations of GeO_6. Most of the bands in the third pressure region are characterized by a lower value of the coefficients of change in the wavenumber values than in the second region. After decompression, all intense bands (υ3, υ6, υ8, υ12, υ15, and υ17) returned to the initial position of the Raman shift. Also, only minor changes were observed in the Raman spectra of $GaGeO_3OH$ compared with the initial spectra under standard conditions. In the Raman spectra of the sample "after high pressure", there is a decrease in the intensity of all bands and an almost complete disappearance of the "shoulder bands" (υ7, υ9, υ18 and υ19) compared with the initial sample "before high pressure". This phenomenon may be related to the amorphization of the sample under the influence of pressure, a similar phenomenon has been observed when pressure is applied to other compounds (e.g. Ruiz-Fuertes et al., 2016). Previous work on the stability of the structural characteristics of the $AlSiO_3OH$ phase at high pressures showed that the *b* axis is the most compressible direction, and the β angle decreases to 16 GPa (Schulze et al., 2018). This is due to the fact that the length of the Si-O4 bond decreases, strengthening it up to a pressure of 16 GPa and at the same time weakening the O4-H bond. In our case, we observed the same effect for the GeO_6 (υ17) valence band; in all three pressure regions, this band has the highest value of $\partial\upsilon/\partial$P, which indicates a stronger compression of the Ge···O bond length compared to the others.

Table 2. Frequency shifts ($\partial\upsilon/\partial P$, cm^{-1}/GPa) of Raman bands of $GaGeO_3OH$.

υ#	Frequency shifts $\partial\upsilon/\partial P$, cm^{-1}/GPa		
	I	II	III
υ 3	0.77 (0.06)	0.81 (0.06)	0.42 (0.01)
υ 4*	0.24 (0.03)	-0.04 (0.05)	Not observed
υ 5*	0.82 (0.16)	1.26 (0.10)	Not observed
υ 6	0.62 (0.17)	1.51 (0.12)	0.97 (0.06)
υ 7*	1.18 (0.06)	Not observed	Not observed
υ 8	1.23 (0.12)	2.06 (0.04)	1.39 (0.08)
υ 9*	-0.07 (0.12)	1.70 (0.04)	Not observed
υ 10*	1.14 (0.34)	Not observed	Not observed
υ 11*	3.09 (0.51)	Not observed	Not observed
υ 12	1.10 (0.16)	2.31 (0.09)	2.37 (0.05)
υ 13	3.29 (0.18)	0.80 (0.08)	0.50 (0.02)
υ 14	-0.88 (0.28)	0.51 (0.06)	2.10 (0.08)
υ 15	0.65 (0.20)	2.82 (0.14)	1.98 (0.04)
υ 16*	1.10 (0.08)	0.88 (0.41)	Not observed
υ 17	3.98 (0.28)	3.89 (0.15)	2.06(0.24)

* - shoulder bands.

Conclusions. *In situ* high pressures Raman spectroscopic study of a new $GaGeO_3OH$ phase (an analog of the Egg $AlSiO_3OH$ phase) up to ~ 30 GPa was made. A change in the spectral patterns of the Raman with a change in the values of the coefficient ($\partial\upsilon/\partial$P), accompanied by the disappearance of several bands at pressures of ~ 4 GPa and ~ 14 GPa, indicates possible structural transformations. The

band corresponding to the GeO6 valence oscillation is characterized by the highest coefficient ($\partial\upsilon/\partial P$), which indicates the most compressible Ge···O bond in the entire pressure range up to ~ 30 GPa.

Acknowledgments

This research was financially supported by the Russian Science Foundation, grant number 24-27-00078.

References

Belokoneva E.L. The structures of new germanates, gallates, borates, and silicates with laser, piezoelectric, ferroelectric, and ion-conducting properties // Russian Chemical Reviews. 1994. V. 63. P. 533–549. https://doi.org/10.1070/rc1994v063n07abeh000103.

Bu X., Feng P., Gier T.E., Zhao D., Stucky G.D. Hydrothermal synthesis and structural characterization of zeolite-like structures based on gallium and aluminum germanates // Journal of the American Chemical Society. 1998. V. 120. P. 13389–13397. https://doi.org/10.1021/ja983042k.

Eggleton R.A., Chappell B.W. The crystal structure of stilpnomelane. Part III: Chemistry and physical properties // Mineralogical Magazine. 1978. V. 42. P. 361–368. https://doi.org/10.1180/minmag.1978.042.323.06

Finger L.W., Hazen R.M. Systematics of High-Pressure Silicate Structures // Reviews in Mineralogy and Geochemistry. 2000. V. 41. P. 123–155. https://doi.org/10.2138/rmg.2000.41.5.

Fukuyama K., Ohtani E., Shibazaki Y., Kagi H., Suzuki A. Stability field of phase Egg, $AlSiO_3OH$ at high pressure and high temperature: Possible water reservoir in mantle transition zone // Journal of Mineralogical and Petrological Sciences. 2017. V. 112. P. 31–35. https://doi.org/10.2465/jmps.160719e.

Lipina O.A., Surat L.L., Chufarov A.Y., Tyutyunnik A.P., Enyashin A.N., Baklanova I. V., Belova K.G., Baklanova Y. V., Zubkov V.G. Structural, electronic, and optical studies of $BaRE_2Ge_3O_{10}$ (RE = Y, Sc, Gd-Lu) germanates with a special focus on the $[Ge_3O_{10}]_8$-geometry // CrystEngComm. 2019. V. 21. P. 6491–6502. https://doi.org/10.1039/c9ce01282f.

Litvin Y.A., Physico-chemical studies of the melting of the Earth's deep substance // Science. 1991. Vol. 312. Moscow.

Luo H., Fang L., Xiang H., Tang Y., Li C. Two novel low-firing germanates $Li_2MGe_3O_8$ (M = Ni, Co) microwave dielectric ceramics with spinel structure // Ceramics International. 2017. V. 43. P. 1622–1627. https://doi.org/10.1016/j.ceramint.2016.10.107.

Mi Z. Strength, Elasticity and Phase Transition Study on NaCl and MgO-NaCl Mixture to Mantle Pressures // The University of Western Ontario, 2013.

Michel D., Colomban P., Abolhassani S., Voyron F., Kahn-Harari A. Germanium Mullite: Structure and Vibrational Spectra of Gels, Glasses and Ceramics // Journal of the European Ceramic Society. 1996. V. 16. P. 161–168. https://doi.org/10.1016/0955-2219(95)00145-X.

Rao R., Rao A.M., Xu B., Dong J., Sharma S., Sunkara M.K. Blueshifted Raman scattering and its correlation with the [110] growth direction in gallium oxide nanowires // Journal of Applied Physics. 2005. 98. https://doi.org/10.1063/1.2128044

Reid A.F., Ringwood A.E. The crystal chemistry of dense M_3O_4 polymorphs: High pressure Ca_2GeO_4 of K_2NiF_4 structure type // Journal of Solid State Chemistry. 1970. V. 1. P. 557–565. https://doi.org/10.1016/0022-4596(70)90142-8.

Ringwood A.E., Seabrook M. High-pressure phase transformations in germanate pyroxenes and related compounds // Journal of Geophysical Research. 1963. V. 68. P. 4601–4609. https://doi.org/10.1029/jz068i015p04601.

Ringwood A.E. Phase transformations and the constitution of the mantle // Physics of the Earth and Planetary Interiors. 1970. V. 3. P. 109–155. https://doi.org/10.1016/0031-9201(70)90047-6.

Rudolph W.W., Pye C.C., Irmer G. Study of gallium(III) nitrate hydrate and aqueous solutions: Raman spectroscopy and ab initio molecular orbital calculations of gallium(III) water clusters // Journal of Raman Spectroscopy. 2002. V. 33. P. 177–190. https://doi.org/10.1002/jrs.842

Ruiz-Fuertes J., Gomis O., León-Luis S.F., Schrodt N., Manjón F.J., Ray S., Santamaría-Pérez D., Sans J.A., Ortiz H.M., Errandonea D., Ferrer-Roca C., Segura A., Martínez-García D., Lavín V., Rodríguez-Mendoza U.R., Muñoz A. Pressure-induced amorphization of $YVO_4:Eu^{3+}$ nanoboxes // Nanotechnology. 2016. V. 27. P. 25701. https://doi.org/10.1088/0957-4484/27/2/025701.

Schulze K., Pamato M.G., Kurnosov A., Ballaran T.B., Glazyrin K., Pakhomova A., Marquardt H. High-pressure single-crystal structural analysis of $AlSiO_3OH$ phase egg // American Mineralogist. 2018. V. 103. P. 1975–1980. https://doi.org/10.2138/am-2018-6562

Shi F., Qiao H. Influence of hydrothermal reaction time on crystal qualities and photoluminescence properties of β-Ga_2O_3 nanorods // Journal of Materials Science: Materials in Electronics. 2020. V. 31. P. 20223–20231. https://doi.org/10.1007/s10854-020-04542-w

Solomatova N.V., Caracas R., Bindi L., Asimow P.D. Ab initio study of the structure and relative stability of $MgSiO_4H_2$ polymorphs at high pressures and temperatures // American Mineralogist. 2022. V. 107. P. 781–789. https://doi.org/10.2138/am-2021-7937

Spivak A. V. , Iskrina A. V. , Setkova T. V., Khasanov S.S., Kuzmin A.V., Zakharchenko E.S., Kvas P.S., Virus A.A. Synthesis and high pressure stability of novel $GaGeO_3OH$ compound - analog of phase Egg $AlSiO_3OH$ // Journal of Physics and Chemistry of Solids. 2025. V. 203. P. 112740.

Thomas S.M., Koch-Müller M., Kahlenberg V., Thomas R., Rhede D., Wirth R., Wunder B. Protonation in germanium equivalents of ringwoodite, anhydrous phase B, and superhydrous phase B // American Mineralogist. 2008. V. 93. P. 1282–1294. https://doi.org/10.2138/am.2008.2739.

Wirth R., Vollmer C., Brenker F., Matsyuk S., Kaminsky F. Inclusions of nanocrystalline hydrous aluminium

silicate “Phase Egg” in superdeep diamonds from Juina (Mato Grosso State, Brazil) // Earth and Planetary Science Letters. 2007. V. 259. P. 384–399. https://doi.org/10.1016/j.epsl.2007.04.041

Xue X., Kanzaki M., Fukui H., Ito E., Hashimoto T. Cation order and hydrogen bonding of high-pressure phases in the Al_2O_3-SiO_2-H_2O system: An NMR and Raman study // American Mineralogist. 2006. V. 91. P. 850–861. https://doi.org/10.2138/am.2006.2064.

Zhang J.H., Kong F., Xu X., Mao J.G. Crystal structures and second-order NLO properties of borogermanates // Journal of Solid State Chemistry. 2012. V. 195. P. 63–72. https://doi.org/10.1016/j.jssc.2011.12.045.

Kotelnikov A.R., Suk N.I., Kotelnikova Z.A., Akhmedzhanova G.M., Drozhzhina N.A. Feldspars and their solid solutions: an experimental study. *UDC 550.89:549.07*

IEM RAS, Chernogolovka, Moscow region (kotelnik1950@yandex.ru)

Abstract. At a temperature of 500-900°C and a pressure of 1-3 kbar, solid solutions of feldspars of various compositions and their cation-exchange reactions with solutions were studied. Based on experimental data, Margules parameters were calculated to describe excess mixing energies of solid solutions and unit cell parameters were refined. A comparison with previously studied feldspars was made. Empirical dependencies for calculating the energy parameters of the Margules model and unit cell volumes for various minerals with a feldspar structure were proposed.

***Keywords**: feldspars, synthesis, solid solutions, thermodynamic functions, crystallochemical parameters*

The reactions of cation exchange of solid solutions of feldspars with water-salt fluids were studied experimentally at temperature of 500-900 °C and pressure of 1-3 kbar. Feldspars with isomorphic substitutions of such elements as Na, K, Rb, Ca, Sr, Ba, B, Al, Ga, Fe^{3+}, Si, Ge, P, As were studied. In addition, a method of synthesis of solid solutions of feldspars at different temperatures was used to construct phase diagrams. The methods and results of the experiments are presented in the work (Kotelnikov, 1995). Excess mixing functions of solid solutions of feldspars were calculated based on original (Kotelnikov, 1995; Kroll H., et al., 1995) and literary data. Data on the values of excess mixing functions of solid solutions allow for comparison for a wide range of the studied feldspars and feldspathoids. The magnitudes of deviation from ideality can be conveniently estimated using the integrated values of G^e and V^e (Kotelnikov, 1995), which are obtained by integrating the values of the redundant functions:

$$G^e_{int} = {}_0\int^1 G^e dX_i; \quad (1)$$

$$V^e_{int} = {}_0\int^1 V^e dX_i; \quad (2)$$

where Xi – mole fraction of the i-th minal of feldspars.

These integrated values allow comparison of different solid solutions of framework aluminosilicates regardless of the type of isomorphic substitutions. At the same time, the G^e_{int} value can only be used to compare the total deviation of solid solutions from ideality. For thermodynamic calculations, the values of the Margules model parameters, or numerical values of the activity coefficients, are used. To compare deviations from ideality of different solid solutions, these values (W^G1, W^G2) had to be reduced to the same temperature. This was done by generalizing the literature data of various researchers. Table 1 shows the coefficients of the polynomials of the dependences of the Margules parameters on temperature: $W^G1,2 = A + B\times T + C\times T^2$. It was previously shown (Kotelnikov et al., 2021) that the values (<T-O>) and R_i^T for feldspars are in a linear relationship:

$$(<T\text{-}O>) = 1.2596 + 0.89324\times(R_i^T)\ [Å]. \quad (3)$$

The R_i^T value is the average size of a cation in a tetrahedral position of the feldspar crystal structure. Therefore, it is possible to calculate the average <T-O> bond lengths for feldspar structures based on the average size of a cation in a tetrahedral position. To evaluate the properties of feldspar solid solutions, it is convenient to use the parameter $A3 = \Delta Ri\times[<T\text{-}O>]^3$, (Kotelnikov, 1995).

Since the G^e_{int} values for all studied feldspar solid solutions have positive values regardless of the isomorphism type, the absolute values of A3 were used to find the dependencies. For solid solutions with anorthite structure (Ca-Sr; Sr-Ba and Ca-Ba feldspars), the value $A3 = 2\times(\Delta R_i)\times[R_i^T]^3$, which is due to the doubling of the lattice parameter of the anorthite type.

The dependence of the G^e_{int} values (750°C) on the A3 value is described by the following regression equation:

$$G^e_{int} = -0.1309+1.8508\times A3;\ S_x=0.36;\ V_x=17\%;\ E_x=0.17;\ E_x(\text{relative})=8\% \quad (4)$$

For the parameters of the Margules model (at 750°C), the following dependencies on the value of A3 were calculated:

$$W^G1 = -0.2230+9.6265\times A3;\ S_x=3.2;\ V_x=28\%;\ E_x=1.6;\ E_x(\text{relative})=14\% \quad (5)$$

$$W^G2 = -2.246+13.1489\times A3;\ S_x=3.3;\ V_x=24\%;\ E_x = 1.6;\ E_x(\text{relative})=12\% \quad (6)$$

Thus, there is a clear connection between the values of excess energies and crystallochemical parameters. The values of the radii of cations in the tetrahedral position and isomorphic cations allow us to estimate the degree of non-ideality of solid solutions of various feldspars in the temperature range of 500-850°C.

Conclusions

1. For various solid solutions of feldspar, the temperature dependences of the Margules coefficients were calculated to describe the excess mixing energies of the solid solutions.

2. The quantitative relationship between the Margules parameters (W^G1 and W^G2) and the crystal-chemical parameters of the feldspar solid solutions was shown.

Table 1. Values of the polynomial coefficients for calculating the Margules parameters (of the type $W^G1,2=a + b\times TK + c\times(TK)^2$) of solid solutions of feldspars

System Fsp	Isomorphism	a (W^G1)	b	c	a (W^G2)	b	c
Na-Ca-Al-Si	Na-Ca	89.7000	-0.14300	0.000060	84.1800	-0.14250	0.000060
Na-Ca-Ga-Si	Na-Ca	-1.4750	0.00106	-	10.6370	-0.00290	-
Na-Sr-Al-Si	Na-Sr	20.8380	-0.01340	-	27.4050	-0.01760	-
Na-Ba-Al-Si	Na-Ba	15.6300	-0.00512	-	22.0500	-0.00855	-
K-Ca-Al-Si	K-Ca	65.023	-0.0397	-	51.902	-0.0345	-
K-Sr-Al-Si	K-Sr	31.0600	-0.01860	-	40.2500	-0.02960	-
K-Ba-Al-Si	K-Ba	28.8100	-0.02380	-	49.5100	-0.04461	-
Rb-Ba-Al-Si	Rb-Ba	8.870	-0.00305	-	12.2060	-0.00460	-
Ca-Sr-Al-Si	Ca-Sr	60.0360	-0.04192	-	59.7260	-0.04169	-
Sr-Ba-Al-Si	Sr-Ba	26.4190	-0.01601	-	26.2810	-0.01590	-
Ca-Ba-Al-Si	Ca-Ba	81.0700	-0.05500	-	81.8200	-0.04370	-
Na-K-Al-Si	Na-K	21.1000	-0.01010	-	31.0500	-0.01380	-
Na-K-Ga-Si	Na-K	19.6000	-0.00875	-	31.8600	-0.01399	-
Na-Rb-Al-Si	Na-Rb	110.8000	-0.09170	-	148.9000	-0.11850	-
K-Rb-Ga-Si	K-Rb	7.1390	-0.00345	-	6.8640	-0.00320	-
Na-K-Al-Ge	Na-K	30.7200	-0.01400	-	30.9400	-0.00600	-
Na-B-Al-Si	B-Al	66.1370	-0.05464	-	38.4600	-0.02828	-
Ca-Ba-Al-Ge	Ca-Ba	65.0820	-0.04400	-	44.5230	-0.02535	-
K-Rb-Al-Si	K-Rb	9.9950	-0.00630	-	9.9950	-0.00630	-

The work was supported by the FMUF-2022-0002 program of the IEM RAS

.

References

Kotelnikov A.R. Isomorphism in framework aluminosilicates. Abstract. diss. … doc. geol-min. sciences. M.: MSU. 1995. 36 p.

Kotelnikov A.R., Suk N.I., Akhmedzhanova G.M., Kotelnikova Z. A. Experimental Study of Cation-Exchange Equilibria of Solid Solutions of Gallium Feldspars $(Na,K)GaSi_3O_8$ with Water–Salt Fluid (NaCl–KCl–H_2O) at 550°C and 1.5 Kbar. Petrology. 2021. V. 29. No. 5. P. 561–574.

Kroll H., Kotelnikov A.R., Goettlicher J., Valyashko E.V. (K,Sr)-feldspar solid solutions: the volume behaviour of heterovalent feldspars. Eur. J. Mineral. 1995. V. 7. P. 489–499.

Kotelnikov A.R., Korneeva A.A., Kosova S.A., Suk N.I., Drozhzhina N.A. Synthesis of feldspars with gallium and germanium. *UDC 550.89:549.07*

IEM RAS, Chernogolovka, Moscow region
kotelnik1950@yandex.ru

Abstract. Feldspars containing gallium and germanium were synthesized by pyrosynthesis (at 1300°C) and hydrothermal recrystallization (at 650°C and P=2 kbar). Experiments on cation exchange equilibria with 1M $SrCl_2$ solution were conducted at 750 and 650°C (P=2 kbar). Their solid solutions were synthesized. The unit cell parameters of the synthesized feldspars and their solid solutions were clarified. These feldspars were synthesized for the first time.

***Keywords**: synthesis, feldspars, gallium, germanium, solid solutions*

Gallium- and germanium-containing feldspars were synthesized from stoichiometric mixtures of carbonates and oxides, pre-annealed at 1300°C for 12 hours. Then, hydrothermal synthesis of feldspars was carried out from pyrosynthetic material at 650 and 750°C and a pressure of 2 and 3 kbar. Pyrosynthetic samples were placed in platinum (or gold) ampoules, into which a small amount of water (~10 wt.%) was

poured. The duration of the experiments was 12-21 days. After the experiments, the samples were studied using microprobe and X-ray analysis.

The compositions of the synthesized solid products of the experiments were determined by the method of local X-ray spectral microanalysis using a Tescan Vega II XMU scanning electron microscope (Tescan, Czech Republic) equipped with an INCA Energy 450 X-ray spectral microanalysis system with energy-dispersive (INCAx-sight) and crystal-diffraction (INCA wave 700) X-ray spectrometers (Oxford Instruments, England) and the INCA Energy+ software platform. The analysis conditions using only an energy-dispersive spectrometer were as follows: accelerating voltage of 20 kV, current of absorbed electrons on Co of 0.3 nA, analysis time at a point of 70 s. X-ray study of solid solutions of gallium-containing alkali feldspars was carried out on an HZG-4 and "Bruker" diffractometer in the continuous scanning mode. Spectral-purity silicon (a=5.4307 [Å]) was used as an internal standard.

Table 1. Parameters of unit cells of gallium- and germanium-containing feldspars

Feldspar	a [Å]	b [Å]	c [Å]	α [°]	β [°]	γ [°]	V [Å^3]	n
$NaAlGe_3O_8$	8.387(1)	13.292(2)	7.281(1)	94.28(1)	115.97(1)	90.66(1)	726.8(3)	58
$KAlGe_3O_8$	8.854(2)	13.842(2)	7.315(2)	90.0	115.48(1)	90.0	809.3(3)	40
$CaAl_2Ge_3O_8$	8.289(2)	12.695(2)	7.309(1)	93.43(2)	116.67(2)	93.31(1)	682.9(4)	41
$CaAlGaSi_2O_8$	8.217(1)	12.940(1)	7.121(1)	93.02(1)	115.74(1)	91.29(1)	680.2(2)	70
$BaAlGaSi_2O_8$	8.661(1)	13.105(1)	7.232(1)	90.0	114.57(1)	90.0	746.6(3)	60
$Ca_{0.6}Sr_{0.4}AlGaSi_2O_8$	8.309(1)	13.014(2)	7.170(1)	91.90(1)	116.13(1)	91.44(1)	695.1(2)	56
$Ca_{0.5}Sr_{0.5}AlGaSi_2O_8$	8.347(2)	13.015(2)	7.134(1)	91.95(1)	115.68(1)	91.09(1)	697.5(3)	49
$CaAlGaSiGeO_8$	8.233(2)	13.456(1)	7.191(1)	93.10(1)	115.18(1)	91.79(1)	718.6(3)	54
$SrAlGaSiGeO_8$	8.482(2)	13.367(2)	7.228(2)	90.0	115.11(1)	90.0	742.1(4)	37
$BaAlGaSiGeO_8$	8.746(2)	13.266(2)	7.259(2)	90.0	114.85(1)	90.0	764.3(4)	52

The polygonal method of correction of X-ray reflections was used (Kroll et.al., 1995; Kotelnikov, 1995). The obtained results allowed us to calculate the unit cell parameters of solid solutions. The unit cell parameters (UCP) were refined using 45–103 reflections in the angular range of 6.5–44.5° (Θ). The parameters were calculated using the LCC, PUDI, and MINCRYST programs (Burnham, 1991; Chichagov, 1994). The UCP values are given in Table 1.

In addition to hydrothermal synthesis, the method of cation exchange equilibria was used: $CaAlGaSi_2O_8 + SrCl_2(aq) = SrAlGaSi_2O_8 + CaCl_2(aq)$. This method allowed us to obtain solid solutions of feldspars with the replacement of calcium by strontium. The UCP of the solid solutions are also given in Table 1. The data obtained are useful for studying the crystallochemical features of solid solutions of framework aluminosilicates and developing ideas about the geochemistry of rare elements in the earth's crust.

The work was supported by the FMUF-2022-0002 program of the IEM RAS.

References

Burnham C.W. Least-squares refinement of crystallographic lattice parameters for IBM PC/XT/AT and compatibles. Cambridge MA02138: Harward University. 1991 (program description) 24 p.

Chichagov A.V. Information-calculating system on crystal structure data of minerals (MYNCRYST). Materials Science Forum. 1994.Volks 166–169. Trans. Tech. Publications. Switzerland. P. 187–192.

Kotelnikov A.R. Isomorphism in framework aluminosilicates. Abstract. diss. … doc. geol-min. sciences. M.: MSU. 1995. 36 p.

Kroll H., Kotelnikov A.R., Goettlicher J., Valyashko E.V. (K,Sr)-feldspar solid solutions: the volume behaviour of heterovalent feldspars. Eur. J. Mineral. 1995. V. 7. P. 489–499.

Kovalskaya T.N.[1], Ermolaeva V.N.[1,2], Kovalskiy G.A.[1], Varlamov D.A.[1,3], Chukanov N.V.[3], Chaychuk K.D.[1], Ermolaev D.N.[1] Zircono- and titanosilicates - indicators of alkalinity in alkaline pegmatites (by experimental data).

[1] – IEM RAS, Chernogolovka [2] – GEOKHI RAS, Moscow
[3] – FRC PCP MC RAS, Chernogolovka
tatiana76@iem.ac.ru

Abstract. At temperature 600 °C and pressure 2 kbar, zircon- and titanosilicates were synthesized in the presence of fluids of varying alkalinity. Such parageneses are observed in postmagmatic formations of the Khibiny and Lovozero ultra-agpaitic complexes. The duration of the experiments was 10 days. The following mineral-like

phases were diagnosed in the experimental products using electron probe microanalysis and X-ray fluorescence: minerals of the eudialyte group, minerals of the lovozerite group, parakeldyshite, occurring in ultra-alkaline postmagmatic formations.

Keywords: *synthesis, zirconosilicates, eudialyte, lovozerite, lowenite, postmagmatic processes, alkaline massifs, alkaline fluid.*

Previously, in order to obtain information on the conditions of zirconium and titanosilicate formation, as well as to study the effect of the fluid regime on the composition of the forming phases, a team of authors conducted a series of experiments on the synthesis of zirconium and titanosilicates in alkaline conditions under various physicochemical conditions (solutions of NaCl, NaF, NaOH, Na_2CO_3 of various concentrations were used as fluids) (Kovalskaya et al., 2023; Kovalskaya et al., 2024). The experiments were carried out in hermetically sealed platinum ampoules on a high gas pressure unit (HGU) and hydrothermal units (UVD-10000) designed by the IEM RAS, at a temperature of 500 - 600 ° C and a pressure of 2 kbar. The sample: solution ratio was 10: 1. The duration of the experiments varied from 10 to 21 days. The experimental products were studied by electron probe microanalysis, X-ray diffraction and IR spectroscopy. The results of the experiments indicate the influence of the fluid regime on the composition of the crystallizing phases under the same conditions of temperature and pressure. During crystallization of zirconium silicates in a less alkaline solution (1M NaF, 1M NaCl with 0-10% NaOH), growth of zirconium silicates (eudialyte, parakeldyshite, lovenite and its Fe analogue, burpalite, zircon) is observed, and in a more alkaline solution (1M NaF with 20% NaOH), lueshite and fluoride (F analogue of lakargiite $CaZrF_6$) are formed. In the synthesis of titanosilicates, the addition of 15% NaOH and 10% Na_2CO_3 to 1M NaCl does not significantly affect the crystallization of mineral phases (joint growth of lorenzenite and lueshite is observed everywhere with some variations of other associated phases - titanite, pectolite and serandite in the first case, titanite in the second case and schisolite, natisite (in the third). Recently, experiments were carried out on the synthesis of zirsinalite. Zirsinalite $Na_6(Ca,Mn,Fe)ZrSi_6O_{18}$, was discovered in the Khibiny alkaline massif (Fig. 1), and was found in several points of the Lovozero massif. Zirsinalite from Mount Karnasurt has been studied in most detail, where it forms colorless rims and pseudomorphs on eudialyte and, in turn, is replaced by lovozerite; it associates with natrosilite, aegirine, analcime, sodalite, nepheline, feldspar, cancrinite, natrolite, villiaumite, thermonatrite, lomonosovite, woonnemite, kazakovite, etc. (Pekov, 2001).

Fig. 1. Tsirsinalite (pseudomorphosis on eudialyte) in association with lovozerite, microcline, aegirine, Yukspor mountain, Khibiny alkaline massif, Kola Peninsula**.**

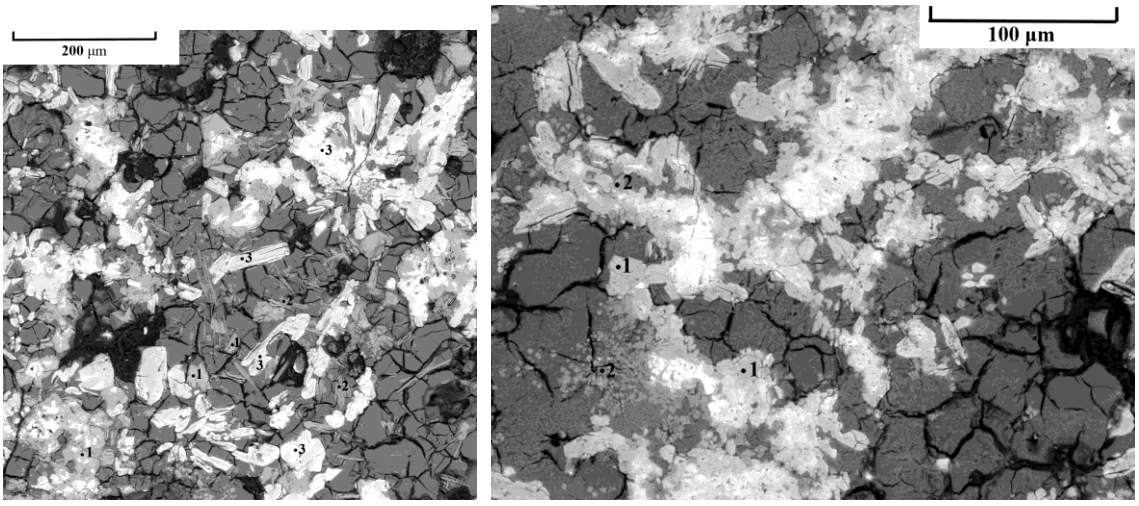

Fig. 2. Results of synthesis of experiment 87. 1 – tsirsinalite, 2 – pectolite, 3 – vlasovite. Back-scattered electron image.
Fig. 3. Results of synthesis of experiment 88. 1 – vlasovite, 2 – pectolite. Back-scattered electron image**.**

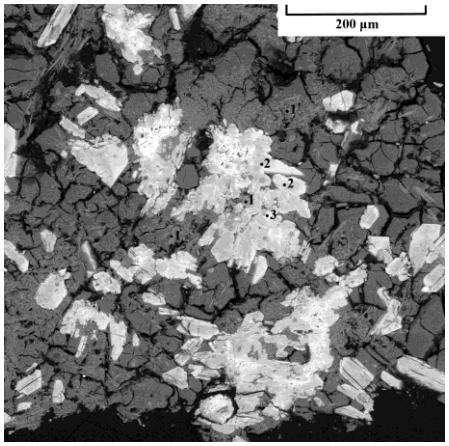

Fig. 4. Results of the synthesis of experiment 89. 1 – pectolite, 2 – vlasovite, 3 – parakeldyshite. Back-scattered electron image.

Table 1. Chemical composition of phases obtained during experiments 87-89.

Compo-nents	Exp. 87			Exp. 88		Exp. 89		
	Vlasovite	Tsirsina-lite	Pectolite	Vlaso-vite	Decationized pectolite with Zr impurity	Vlasovite	Para-keldyshite	Pectolite
weit. %								
Na_2O	12.39	12.51	9.61	12.46	13.76	12.61	17.34	9.80
CaO	bdl	12.56	33.00	bdl	14.67	0.34	0.34	31.99
ZrO_2	29.674	17.12	1.09	29.17	14.71	31.09	42.62	bdl
HfO_{12}	2.16	bdl	bdl	bdl	bdl	bdl	bdl	bdl
SiO_2	55.68	55.45	55.47	56.98	56.40	55.86	37.74	56.67
Nb_2O_5	bdl	bdl	bdl	bdl	bdl	1.88	bdl	bdl
Σ	99.89	97.65	99.16	98.62	99.53	101.78	98.05	98.46
formula coefficients								
Na	1.73	2.63	1.01	1.70	1.42	1.75	1.78	1.00
Ca	0	1.46	1.91	0	0.84	0.03	0.02	1.81
Zr	1.04	0.90	0.03	1.00	0.38	1.08	1.10	0
Hf	0.04	0	0	0	0	0	0	0
Si	4.00	6.00	3.00	4.00	3.00	4.00	2.00	3.00
Nb	0	0	0	0	0	0.06	0	0

The experiments were carried out from a sol-gel of the zirsinalite composition using 10, 20 and 30% NaOH solutions. The experiments were carried out on a hydrothermal setup (UVD-10000) designed by the IEM RAS at a temperature of 550 °C and a pressure of 2 kbar. In experiment 87 with a 10% NaOH solution, vlasovite, decationized zirsinalite and pectolite were formed; in experiment 88 with a 20% NaOH solution, vlasovite and pectolite were formed, and in experiment 89 with a 30% NaOH solution, vlasovite, parakeldyshite and pectolite were formed (Table 1, Figures 2-4).

The infrared spectroscopic study was performed in accordance with the State Assignment theme, state record number AAAA-A19-119092390076-7, and the rest of the work was performed under State Assignment theme FMUF-2022-0002

Kuzyura A.V., Spivak A.V., Setkova T.V., Iskrina A.V., Zakharchenko E.S., Viryus A. A. High-pressure synthesis of Ge-analogues of olivine (α-Mg_2GeO_4) and spinel (γ -Mg_2GeO_4). *UDC 550.4.02, 549.057*

D.S. Korzhinsky Institute of Experimental Mineralogy RAS, Russia, Chernogolovka shushkanova@iem.ac.ru spivak@iem.ac.ru setkova@iem.ac.ru iskrina@iem.ac.ru egorzero@gmail.com allavirus@yandex.ru

Abstract. Geochemical similarity of silicon to germanium allows using germanates as analogues of planetary silicates. In addition, as a rule, germanates undergo similar phase transitions, but at significantly lower pressures than similar silicate minerals. In this regard, a test high-pressure synthesis of Mg-germanates were carried out. Crystals of α-Mg_2GeO_4 olivine with size up to 100 μm were obtained in the $Mg(OH)_2$-$MgCO_3$-GeO_2 system at pressure of 5 GPa and temperature of 900 °C. Crystals of γ-Mg_2GeO_4 spinel with size up to 50 μm were synthesized in the MgO-GeO_2-H_2O system at 7 GPa and 900 °C. Phase identification was carried out using electron probe analysis and Raman spectroscopy.

***Keywords**: HPHT experiments; synthesis; germanium; Ge-analogues of minerals; Raman-spectroscopy*

The geochemical similarity of silicon to germanium allows the use of germanates as analogues of planetary silicates (Dutta et al., 2018; Finger and Hazen, 2000; Reid and Ringwood, 1970; Ringwood, 1970; Stan et al., 2017). Olivine $(Mg,Fe)_2SiO_4$ is the most abundant mineral in the

Earth's upper mantle. A cause of the main seismic boundaries (410 and 520 km) in the upper mantle and the transition zone is the phase transitions of the Mg-rich olivine α-$(Mg,Fe)_2SiO_4$ into wadsleite β-$(Mg,Fe)_2SiO_4$ and ringwoodite γ-$(Mg,Fe)_2SiO_4$ (Ringwood 1991). Synthetic germanium analogues of olivine and spinel α,γ-X_2GeO_4 (X=Mg, Mn, Co....) and their phase transformations have been studied since the 70s of the last century and has not lost its relevance today (Akimoto, 1970; Divya et al., 2024; Dupas-Bruzek et al., 1998; Ross et al., 1987; Shi et al., 2015). Currently solid-phase synthesis is the most available methods of synthesis of Ge-analog for subsequent researches. Olivine (α-Mg_2GeO_4) was synthesized from magnesium and germanium oxides at 1473-1770 K (1-5 days) (Divya et al., 2024; Fiquet et al., 1992; Ross et al., 1987). Spinel (γ-Mg_2GeO_4) can be synthesized at 0.07 GPa and 973-1048 K (5 days) by the hydrothermal method using previously obtained olivine as a starting material (Ross et al., 1987). A high-impact and high-temperature experiment was used to study the phase state of Mn_2GeO_4. The α-modification was synthesized at 2.5-4 GPa, β- at 4-6 GPa, and δ- at 6-7 GPa in the temperature range of 800-1200 °C (Akimoto, 1970). In addition, the kinetic characteristics of the α-$Mg_2GeO_4 \rightarrow \gamma$-$Mg_2GeO_4$ phase transition were estimated at pressure range 0-50 kbar and 25-1100 °C (Lauterjung and Will, 1986). A phase diagram with generalized data on the α-$Mg_2GeO_4 \rightarrow \gamma$-$Mg_2GeO_4$ phase transition at that time was presented by Ross et al. at a pressure up to 4 GPa and a temperature up to 1900 °C (Ross et al., 1987).

In this paper, we give results for high-pressure (5 and 7 GPa) and high-temperature synthesis of two modifications: olivine α-Mg_2SiO_4 and spinel γ-Mg_2GeO_4 for their subsequent using at experimental researches at high pressure.

The synthesis experiments were carried out with using of toroidal anvils press at the D.S. Korzhinsky Institute of Experimental Mineralogy of the Russian Academy of Sciences (IEM RAS) (Litvin, 1991). Magnesium oxides (99.9%), germanium oxide (99.9%), magnesium hydroxide (99.5%) and magnesium carbonate (99.5%) were used as the starting material. Starting sets within the model systems $Mg(OH)_2$-$MgCO_3$-GeO_2 and MgO-GeO_2-H_2O (deionized water) were placed in an Au ampoule. The experiments were carried out at P=5.0 and 7.0 GPa and T=900 °C. The pressure was determined using the standard Bi polymorphism (at 2.55, 2.7, and 7.7 GPa) with an accuracy of ± 0.25 GPa. The temperature was measured and controlled by a thermocouple ($Pt_{70}Rh_{30}/Pt_{94}Rh_6$) with an accuracy of ± 20 °C. After the experiment, the sample was cooled upto 20 °C at a rate of 300 ± 50 °C/sec.

The habitus of the obtained crystals, surface structure, and composition were studied using the Tescan Vega II XMU scanning electron microscope (SEM) with secondary and reflected electron detectors, as well as an energy-dispersive X-ray spectrometer (INCAx-sight) for quantitative analysis. Electron probe X-ray spectral analysis of the studied samples was performed at an accelerating voltage of 20 kV, an absorbed electron current of 0.2 nA, and a probe size of 0.3 microns. The analysis time was 70 seconds. The following standards were used for the quantitative determination of the major elements: for Ge – Ge elementary, for Ga – GaP.

The Raman spectra of the crystals were captured on a setup consisting of an Acton SpectraPro-2500i spectrograph with a Pixis2K CCD detector cooled to -70 °C and an Olympus microscope with a continuous solid-state single-mode laser with a wavelength of 532 nm. The laser beam was focused on the sample using an Olympus 50× lens into a spot with a diameter of ~5 μm. The signal accumulation time was 540 sec (3x180sec). The obtained spectra were processed using of the Fityk 1.3.1 program.

Results of experiments in the system $(Mg(OH)_2$-$MgCO_3)_{50}$-$(GeO_2)_{50}$ are represented by the following phases: olivine α-Mg_2SiO_4, spinel γ-Mg_2GeO_4, and magnesite $MgCO_3$ (Fig.1a). The chemical composition of the obtained phases corresponds to the crystallochemical formulas of these minerals. Ge-olivine forms prismatic crystals up to 100 microns in size with inclusions of Ge-spinel and magnesite. Small (first microns) octahedral single crystals and Ge-spinel twins form local groups in the total fine crystalline mass of magnesium carbonate (fig. 2a). According to Raman spectroscopy data, residual $Mg(OH)_2$ was not detected.

The obtained result on the joint formation of germanium phases α-Mg_2SiO_4 and γ-Mg_2GeO_4 at pressure of 5 GPa and temperature of 900 °C is consistent with data on the kinetics of transformation α-$Mg_2GeO_4 \rightarrow \gamma$-$Mg_2GeO_4$ at 50 kbar and 1100 °C (Lauterjung and Will, 1986).

In the case of using of the MgO-SiO_2 starting system with an excess of H_2O (deionized water) at pressure of 7 GPa and temperature of 900 °C, we have obtained a white fine crystalline powder consisting of crystals of cubic habitus. They are well faceted, octahedral in shape. Twins are often occurs among them, the size of the individuals is up to 20-30 microns (Fig. 1 b). The chemical composition of the resulting phase corresponds to the crystallochemical formula Mg_2GeO_4. According to Raman spectroscopy data, the modification of spinel γ-Mg_2GeO_4 is determined.

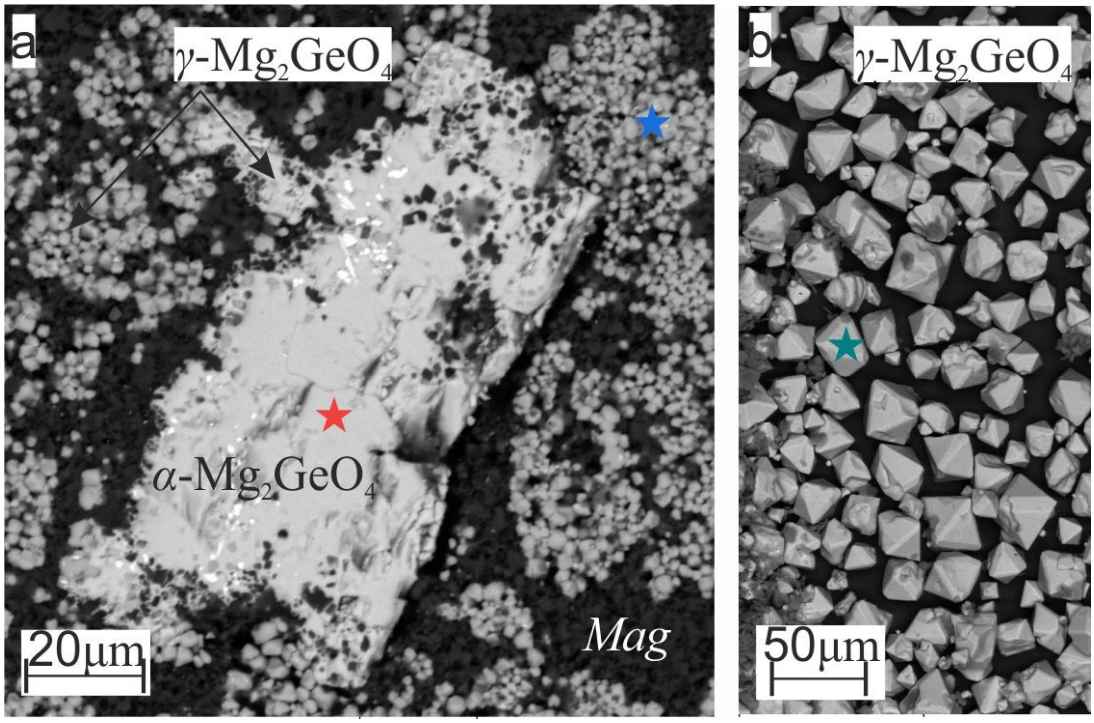

Fig. 1. SEM image of the experimental sample of the (a) $Mg(OH)_2$-$MgCO_3$-GeO_2 system at 5 GPa and 900 °C and (b) MgO-GeO_2-H_2O system at 7 GPa and 900°C. Stars in the SEM image mark the points where the Raman spectra were obtained (see fig. 2). *Mag* – magnesite

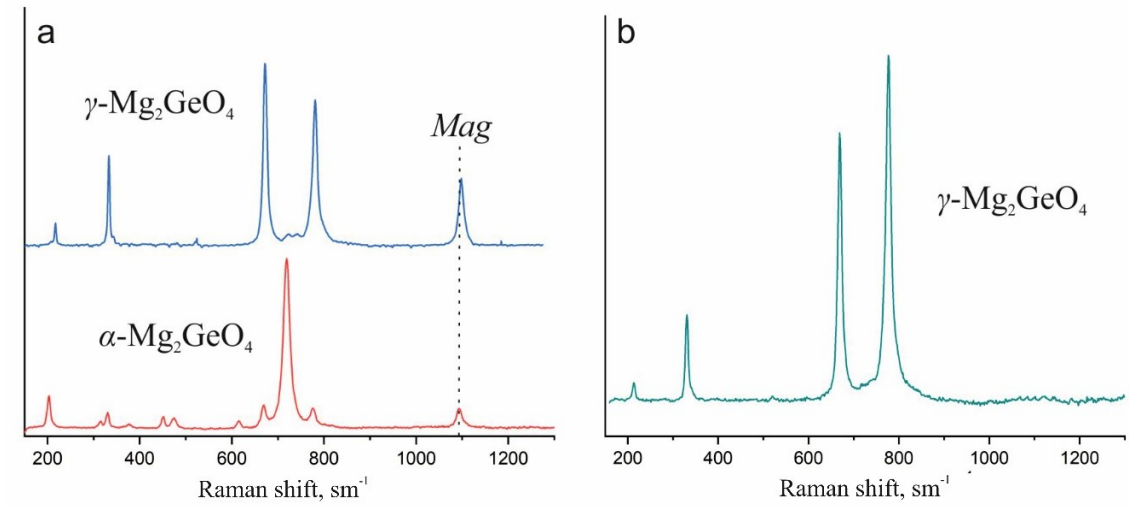

Fig. 2. Raman spectrum of identification of the germanium phase α-Mg_2SiO_4 and γ-Mg_2GeO_4 from the experimental samples: (a) of the $Mg(OH)_2$-$MgCO_3$-GeO_2 system at 5 GPa and 900 °C; (b) of the MgO-GeO_2-H_2O system at 7 GPa and 900°C. The point of obtaining the Raman spectrum is marked with a star in the SEM image (see fig. 1)

Factor group analysis predicts that the olivine structure with *Pnma* symmetry has 36 Raman active modes: 11*Ag* + 11*B*1g + 7*B*2g + 7*B*3g (Cnopnras, 1991). The Raman spectrum of Ge-olivine at standard conditions is characterized by the presence of a low-frequency band group, including lattice vibration modes and deformation modes of the GeO_4 tetrahedron in the range of 150-520 cm^{-1}, and a high-frequency band group at 680-800 cm^{-1}, which correspond to the modes of valence vibrations of the GeO_4 tetrahedron (Reynard et al., 1994). The topology of the obtained Raman spectrum of α-Mg_2SiO_4 is similar to those previously published (Guyot et al., 1986; Reynard et al., 1994; Ross et al., 1987), while certain positions of the Raman bands in this work differ slightly from previously published data, which are in a good agreement (Table 1). In addition, the Raman spectrum of Ge-olivine shows a weak inclusion band of magnesite ~1097 cm^{-1} (Fig. 2a red line).

Table 1. Comparison of the positions of the bands of the Raman spectra of α-Mg_2GeO_4, determined in this work, with the literature data, under standard conditions (cm^{-1}).

The positions of the Raman spectrum bands (cm^{-1}) of α-Mg_2GeO_4				
This work	(Ross et al., 1987)	(Guyot et al., 1986)	(Reynard et al., 1994)	
	152			151
	164			163
179				171
203				229
	278			274
315	298			295
330	337			335
342	354			351
378	398			394
	415			412
451	452			450
475	499			496
512	518			515
669	680	681		678
702	688	688		684
719	710	710		706
736	732	731		729
755	762	763		760
775				776
801	802	801		798

Table 2. Comparison of the positions of the Raman bands of γ-Mg_2GeO_4, determined in this work, with the literature data, at standard conditions (cm^{-1}) .

The positions of the Raman spectrum bands (cm^{-1}) of γ-Mg_2GeO_4					Reference
F_{2g}	E_g	F_{2g}	F_{2g}	A_{1g}	
212	330	552	667	776	This work (fig.1)
213	331	520	667	777	This work (fig.2)
213	342	521	671	779	(Thomas et al., 2008)
213	341	520	669	777	(Ross et al., 1987)

The Ge-spinel γ-Mg_2GeO_4 belongs to the spatial group $Fd\bar{3}m$. The factor group analysis suggests the presence of 42 vibrational modes in the spinels: 3 acoustic and 39 optical ones. However, only five Raman-active vibrational modes with the following symmetries $A_{1g} + E_g + 3F_{2g}$ are acceptable for oxide spinels (Setkova et al., 2022). The positions of the Raman bands of synthetic germanium spinel, determined in this work (fig. 2 a blue line, fig. 2 b green line), are shown in Table 2 and are in accordance with previously published works.

As a result of the carried out test experiments in the system $Mg(OH)_2$ - $MgCO_3$ - GeO_2 at 5 GPa and 900 °C, α-Mg_2GeO_4 olivine crystals up to 100 microns in size were synthesized. γ–Mg_2GeO_4 spinel crystals up to 50 microns in size were synthesized in the MgO-GeO_2-H_2O system at 7 GPa and 900 °C. The phases were identified using electron probe analysis and Raman spectroscopy. The thermobaric crystallization parameters of the experimentally obtained mineral phases are in accordance with the phase diagrams of the MgO-GeO_2 system. At the same time, spectroscopic characteristics are a reliable tool for accurate identification of structural modifications (α-Mg_2GeO_4 and γ-Mg_2GeO_4) obtained at various *PT* experimental conditions.

***Source**: the work was fulfilled under Research program № FMUF-2022-0001 and FMUF-2022-0002 of the Korzhinskii Institute of Experimental Mineralogy*

References:

Akimoto S. High-pressure synth esis of a “modified” spinel and some geophysical implications // Physics of the Earth and Planetary Interiors. -1970. -V. 3. -p. 189–195.

Cnopnras A. Single crystal Raman spectra of forsterite, fayalite, and monticellite // American Mineralogist. -1991. –V. 76, Abe_Anode_SEI.pdf Aurbach_Carbon_solgel.pdf Aurbac.

Divya R.V., Kumar G., Cohen R.E., Tracy S.J., Meng Y., Chariton S., Prakapenka V.B., Dutta R. High-pressure Phase Transition of Olivine-type Mg_2GeO_4 to a Metastable Forsterite-III type Structure and their

Equation of States //American Mineralogist. -2024. - V. 109. -p. 2052–2059.
Dupas-Bruzek C., Tingle T.N., Green H.W., Doukhan N., Doukhan J.C. The rheology of olivine and spinel magnesium germanate (Mg_2GeO_4): TEM study of the defect microstructures // Physics and Chemistry of Minerals. -1998. -V. 25, -p. 501–514.
Dutta R., Tracy S.J., Stan C. V., Prakapenka V.B., Cava R.J., Duffy T.S. Phase stability of iron germanate, $FeGeO_3$, to 127 GPa // Physics and Chemistry of Minerals. -2018. -V. 45. -p. 367–379.
Finger L.W., Hazen R.M. Systematics of High-Pressure Silicate Structures // Reviews in Mineralogy and Geochemistry. -2000. -V. 41. -p. 123–155.
Fiquet G., Gillet P., Richet P. Anharmonicity and high-temperature heat capacity of crystals: the examples of Ca_2GeO_4, Mg_2GeO_4 and $CaMgGeO_4$ olivines // Physics and Chemistry of Minerals. -1992. -V. 18. -p. 469–479.
Guyot F., Boyer H., Madon M., Velde B., Poirier J.P. Comparison of the raman microprobe spectra of $(Mg, Fe)_2SiO_4$ and Mg_2GeO_4 with olivine and spinel structures // Physics and Chemistry of Minerals. - 1986. -V. 13. -p. 91–95.
Lauterjung J., Will G. The kinetics of the olivine-spinel transformation in Mg_2GeO_4 under high pressure and temperature // Physica B+C. -1986. -V.139–140, -p. 343–346.
Reid A.F., Ringwood A.E. The crystal chemistry of dense M_3O_4 polymorphs: High pressure Ca_2GeO_4 of K_2NiF_4 structure type // Journal of Solid State Chemistry. - 1970. -V. 1. -p. 557–565.
Reynard, B., Petit P.-E., Guyot F., Gillet P. Pressure-induced structural modifications in Mg_2GeO_4-olivine: A Raman spectroscopic study // Physics and Chemistry of Minerals. -1994. -V. 20. -p. 556–562.
Ringwood A.E. Phase transformations and the constitution of the mantle // Physics of the Earth and Planetary Interiors. -1970. -V. 3. -p. 109–155.
Ross N.L., Navrotsky A. The Mg_2GeO_4 Olivine-Spinel Phase Transition // Physics and Chemistry of Minerals. -1987. -V. 14. -p. 473–481.
Setkova T. V., Spivak A. V., Borovikova E.Y., Voronin M. V., Zakharchenko E.S., Balitsky V.S., Kuzmin A. V., Sipavina L. V., Iskrina A. V., Khasanov S.S. Synthetic brunogeierite Fe_2GeO_4: XRD, Mössbauer and Raman high-pressure study // Spectrochimica Acta Part A: Molecular and Biomolecular Spectroscopy. -2022. -V. 267. 120597.
Shi F., Zhang J., Xia G., Jin Z., Green H.W. Rheology of Mg_2GeO_4 olivine and spinel harzburgite: Implications for Earth's mantle transition zone // Geophysical Research Letters. -2015. -V. 42. -p. 2212–2218.
Stan C. V., Dutta R., Cava R.J., Prakapenka V.B., Duffy T.S. High-Pressure Study of Perovskites and Postperovskites in the $(Mg,Fe)GeO_3$ System // Inorganic Chemistry. -2017. -V. 56. -p. 8026–8035.
Thomas S.M., Koch-Müller M., Kahlenberg V., Thomas R., Rhede D., Wirth R., Wunder B. Protonation in germanium equivalents of ringwoodite, anhydrous phase B, and superhydrous phase B // American Mineralogist. -2008. -V. 93. - p. 1282–1294.

Verchenko P.A., Setkova T.V., Spivak A.V., Zakharchenko E.S. Synthesis and high-pressure stability of $NaGaGe_2O_6$ with pyroxene structure. *UDC 549.642*

Institute of Experimental Mineralogy named after Academician D.S. Korzhinsky RAS, Chernogolovka, yapoletta@mail.ru

Abstract. Sodium gallium germanate $NaGaGe_2O_6$ was obtained by hydrothermal method at T = 600°C and P = 100MPa. It adopts the structure of the pyroxene-type chain, with monoclinic symmetry and space group C2/*c*, unit cell parameters: *a* = 9.795(3) Å, *b* = 8.844(2) Å, *c* = 5.4543(16) Å, *β* = 104.97(3)°, V = 456.5(2) Å³. Colourless crystals of elongated morphology, ranging in size from 50 to 300 μm were grown. The spectroscopic characteristics of the new compound in the wavelength range of 100-1200 cm⁻¹ have been investigated, including the *in situ* Raman spectroscopy study of the high-pressure behavior of $NaGaGe_2O_6$ at pressures up to ~26 GPa. Possible structural transformations were established at pressures of ~6 GPa and ~19 GPa.

***Keywords**: pyroxenes; Raman spectroscopy; hydrothermal synthesis; germanium;*

Introduction. Pyroxenes are widespread family of rock-forming minerals. The general formula of pyroxenes and their structural analogues can be represented as $M_2M_1T_2O_6$, where $M2 = Ca^{2+}$, Na^{+}, and Li^{+}; $M1 = Al^{3+}$, Ga^{3+}, Fe^{3+}, Mn^{3+}, V^{3+}, Ti^{3+}, Sc^{3+}, or In^{3+}; and $T = Si^{4+}$, Ge^{4+}. The wide isomorphism of cationic sites accounts for chemical and consequently structural diversity among both natural and synthetic compounds. The crystal structure of pyroxenes is characterized by chains of $[SiO_4]$ tetrahedra oriented along the *c*-axis and connected by bridging oxygen atoms. Two nonequivalent cationic sites, *M*1 and *M*2, are distinguished in the pyroxene structure. Pyroxenes are divided into orthorhombic (orthopyroxenes) and monoclinic (clinopyroxenes) groups, crystallizing in various space groups such as P2/*n*, P*bca*, P21/*c*, and C2/*c*.

The synthesis of new compounds with pyroxene structures, including those, that have no natural analogues, as well as the study of their crystal-chemical characteristics and potential properties, is an important task in experimental mineralogy. One of these compounds is the alkali gallium-germanium pyroxene. The compound $NaGaGe_2O_6$ was previously synthesized (Redhammer, 2014) at high pressure (20 GPa) and temperature (1200°C). Literature data shows that synthetic analogues of other germanium pyroxenes, such as $NaFeGe_2O_6$ (Redhammer et al., 2011), $NaCrGe_2O_6$ (Redhammer et al., 2008; Nenert et al., 2009), $NaVGe_2O_6$ (Emirdag-Eanes & Kolis, 2004), and $NaMnGe_2O_6$ (Chen et al., 2013), are also of scientific interest.

The aim of this work is to establish the conditions for hydrothermal synthesis of an alkali

gallium-germanium-containing pyroxene and to conduct a comprehensive study, including under high pressure, which will expand knowledge of the structural variability and potential applications of pyroxene-structured compounds.

Materials and methods. Hydrothermal synthesis of the Ga-Ge pyroxene was carried out at T = 600°C and P = 100 MPa. The starting mixture consisted of gallium and germanium oxides in a 1:2 molar ratio. Gold capsules with volume of 2 cm³ were filled with the oxide mixture and an alkali solution (8 wt.% NaOH) according to the filling coefficient (Naumov, 1971), sealed, and placed in a high gas pressure apparatus (HGPA). The duration of the experiments was 8 days.

Crystals obtained by hydrothermal synthesis were analyzed using optical (MBS-10) and polarization (Nikon Eclipse LV100pol) microscopes. Powder X-ray diffraction patterns of the synthesized phase were recorded on a Bruker D8 Advance diffractometer. Unit cell parameters were obtained using a single-crystal X-ray diffractometer Xcalibur AtlasS2, Gemini R-CCD. The chemical composition of the samples was determined on polished surfaces with carbon coating using a Tescan Vega II XMU scanning electron microscope equipped with an INCA Energy 450 energy-dispersive spectrometer (EDS).

Raman spectra at ambient conditions were recorded on a Renishaw RM1000 spectrometer equipped with a Leica microscope and a solid-state laser at λ = 532 nm, at 50× magnification with a 100s acquisition time. Studying the pressure effect on silicates and their germanium analogues is important for understanding Earth's interior. Pyroxenes exhibit various phase transitions depending on composition, temperature, and pressure. Therefore, additional studies of the pressure stability of $NaGaGe_2O_6$ were performed by *in situ* Raman spectroscopy. Raman spectra were collected using an Acton SpectraPro-2500i spectrograph with a CCD Pixis2K detector cooled to -70°C and an Olympus microscope with a continuous-wave single-mode solid-state laser at 532 nm. The laser beam was focused on the sample through an Olympus 50× objective to a spot of ~5 μm diameter. The excitation intensity at the sample was ~0.7 mW. Signal accumulation time was 540 s (3×180 s). A diamond anvil cell with 16-sided anvils and 250 μm culet size was used; the gasket hole diameter was 100 μm. NaCl served as the pressure-transmitting medium. Pressure was determined using the ruby fluorescence scale. Raman spectra of the alkali gallium-germanium pyroxene were obtained up to ~26 GPa with 0.25–1 GPa increments. Spectra were processed using Fityk 1.3.1 software.

Results and Discussion. Colourless crystals obtained by hydrothermal synthesis ranged from 50 to 300 μm (Fig. 1*a,b*). They formed elongated aggregates with prismatic and columnar shapes, exhibiting perfect cleavage along the prism and fracture angles of approximately 90°.

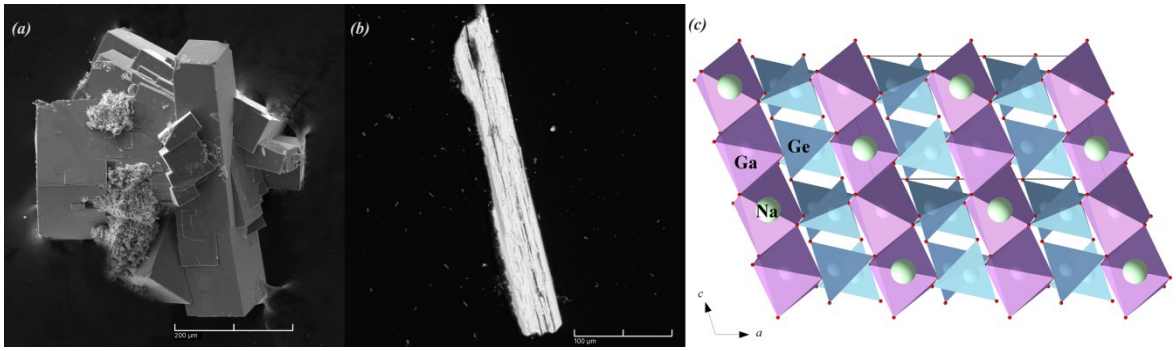

Fig. 1. SEM images of synthesized $NaGaGe_2O_6$ crystals as aggregates (a) and single crystal (b); (c) projection of the $NaGaGe_2O_6$ crystal structure on the *ac* plane, visualized in Diamond software based on structural data (Redhammer, 2014).

Phase identification was performed based on powder diffraction data and Raman spectra. According to electron microprobe analysis at 30 points, the chemical composition is uniform throughout the sample with 62.55 wt.% GeO_2, 28.87 wt.% Ga_2O_3, and 8.53 wt.% Na_2O. The crystal-chemical formula of the synthesized crystals is close to the ideal $NaGaGe_2O_6$. The compound crystallizes in the monoclinic system, space group C2/c (Fig. 1*c*). Unit cell parameters (Table 1) differ from natural analogues (Cameron, 1973) toward larger values. This is explained by the incorporation of larger gallium cations (r_{Ga} = 0.62 Å, compared to Al and Fe^{3+} radii of 0.53 Å and 0.55 Å, respectively) in the *M*1 site and substitution of silicon atoms (r_{Si} = 0.26 Å) by germanium ions (r_{Ge} = 0.56 Å) in the *T* site. Thus, the unit cell volume of the Ga-Ge analogue is ~13% larger than that of natural jadeite. The parameters slightly differ from those refined by Redhammer (2014), possibly due to different *P-T* synthesis conditions.

Table 1. Crystallographic characteristics of Ga-Ge pyroxene analogue, aegirine, and jadeite.

$NaGaGe_2O_6$ (This study)	$NaGaGe_2O_6$ Redhammer, 2014)	Aegirine $NaFeSi_2O_6$ (Cameron, 1973)	Jadeite $NaAlSi_2O_6$ (Cameron, 1973)
a = 9.795(3)Å;	a = 9.9279 (9) Å;	a = 9.658(2)Å,	a = 9.423(1) Å,
b = 8.844(2) Å;	b = 8.8550 (8) Å;	b = 8.795(2)Å,	b= 8.564(1) Å,
c = 5.4543(16) Å;	c = 5.4680 (6) Å;	c = 5.294(1)Å,	c = 5.223(1) Å,
β = 104.97(3)°;	β = 107.5419 (11);	β = 107.42(2)°,	β = 107.56(1)°,
V = 456.5(2) Å^3	V = 458.35 (8)Å^3	V = 429.1(1) Å^3	V = 401.8(1) Å^3

The Raman spectrum of synthetic $NaGaGe_2O_6$ was obtained for the first time in the 100–1200 cm^{-1} range (Fig. 2). According to Wang et al. (2001), this range can be divided into five regions: **(I) 1100–800 cm^{-1}** with a strong asymmetric peak near 1000 cm^{-1} and several broad weak shoulders corresponding to non-bridging tetrahedral stretching modes; **(II) 800–600 cm^{-1}** with an intense doublet or an asymmetric single peak near 670 cm^{-1}, assigned to T-O_{br}-T stretching/bending modes (where O_{br} is the bridging oxygen connecting tetrahedra in the pyroxene chain); **(III) 600–450 cm^{-1}** with overlapping moderate peaks related to O-T-O bending vibrations; **(IV) 450–300 cm^{-1}** with intense overlapping peaks corresponding to internal vibrations of M1 and M2 octahedra, and tetrahedral chain motion and tilting tetrahedra; **(V) <300 cm^{-1}** with several moderate intensity peaks belonging to lattice vibrations.

The number, positions, and relative intensities of peaks vary for pyroxenes with different elemental compositions. For Ga-Ge pyroxene, main peaks shift to lower wavenumbers compared to natural pyroxenes (Guyot et al., 1986) due to substitution of Si^{4+} by heavier Ge^{4+} cations. Si–O bond lengths in silicate tetrahedra typically range from 1.60 to 1.65 Å, while Ge–O distances range from 1.70 to 1.80 Å (Wang et al., 2003). Lower vibrational frequencies in germanates compared to silicates are expected due to both increased atomic mass of the tetrahedral cation and weaker Ge–O bond strength (Guyot et al., 1986). Comparative Raman spectra analysis of aegirine $NaFeSi_2O_6$ (RRUFFID=R040054) and jadeite $NaAlSi_2O_6$ (RRUFFID=R050220) minerals is presented in Table 2.

Table 2. Wavenumbers (cm^{-1}) of observed bands in aegirine $NaFeSi_2O_6$, jadeite $NaAlSi_2O_6$, and $NaGaGe_2O_6$.

	Jadeite	**Aegirine**	**$NaGaGe_2O_6$**	
V	115.1095		113.9578	
	145.5123	135.0515		
		162.0819	160.8453	
		180.9578	176.0314	lattice modes
	204.2876	214.8685	187.6897	
	223.4797			
			234.3336	
IV	**374.8844**	**343.0082**	**307.3967**	
	386.8974	**388.7049**		O-T-O vibrations
	434.1441		**400.5082**	internal vibration modes of M1 и M2
III		499.5865	445.8134	
	525.1625	**544.0054**		O-T-O bending vibrations
	575.677	554.9259	534.2083	
II	**699.2846**	678.7038	**559.5879**	stretching/bending T-O_{br}-T modes,
	778.9329	758.5151	772.4261	internal vibration modes of SiO_4 and GeO_4
I	885.5667	**868.1086**		
		931.236	803.2016	non-bridging tetrahedral stretching modes
	990.8673	**973.2798**	**831.6752**	(SiO_4 and GeO_4)
	1040.244	**1044.524**	**878.0317**	

Raman spectroscopy data under pressures up to 26.08 GPa is shown in Fig. 3. The main Raman bands of $NaGaGe_2O_6$ shift gradually to higher wavenumbers with increasing pressure. At ~6 GPa,

the band at 159 cm^{-1} disappears, and bands at 113, 233, 400, 559, and 878 cm^{-1} change their pressure shift slope. At ~19 GPa, a new band appears at 425 cm^{-1}, and the band in the 113–159 cm^{-1} range disappears. Similar phenomena are observed in some natural pyroxenes such as jadeite (Sakamaki et al., 2012) and spodumene (Jiang et al., 2025). However, no phase transitions up to 8 GPa were detected by *in situ* Raman spectroscopy in natural diopside $CaMgSi_2O_6$ and synthetic $CaCoSi_2O_6$, $CaCoGe_2O_6$, and $CaMgGe_2O_6$ pyroxenes (Tribaudino et al., 2016).

Conclusion. Thus, a structural analogue of pyroxene $NaGaGe_2O_6$ was grown by hydrothermal synthesis at relatively low *P-T* conditions (600°C and 100 MPa). The colorless crystals up to 300 μm in size crystallize in space group *C*2/*c* with unit cell parameters a = 9.795(3) Å, b = 8.844(2) Å, c = 5.4543(16) Å, β = 104.97(3)°, and volume V = 456.5(2) Å³. The Raman spectra of this compound was obtained for the first time and compared with spectra of natural pyroxenes jadeite and aegirine. Pressure stability of the alkali gallium-germanate was studied in the range 0.11–26.08 GPa. Raman spectroscopy indicates possible structural changes in $NaGaGe_2O_6$ at pressures of ~6 GPa and ~19 GPa.

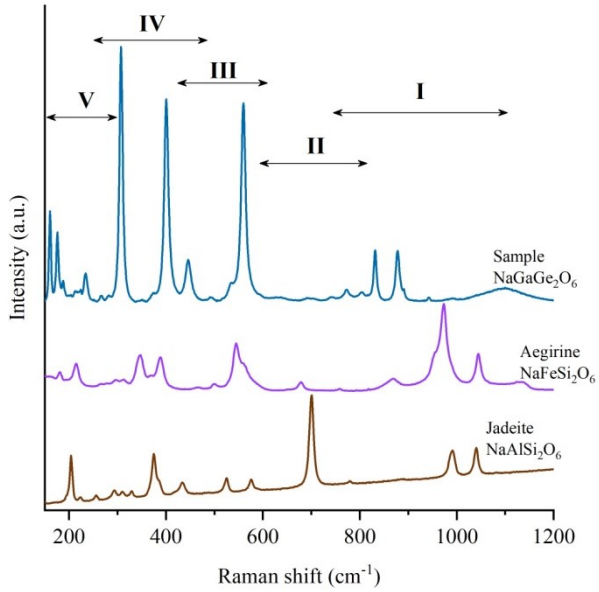

Fig. 2. Unpolarized Raman spectra of synthesized $NaGaGe_2O_6$ crystals compared with natural jadeite (R050220) and aegirine (R040054).

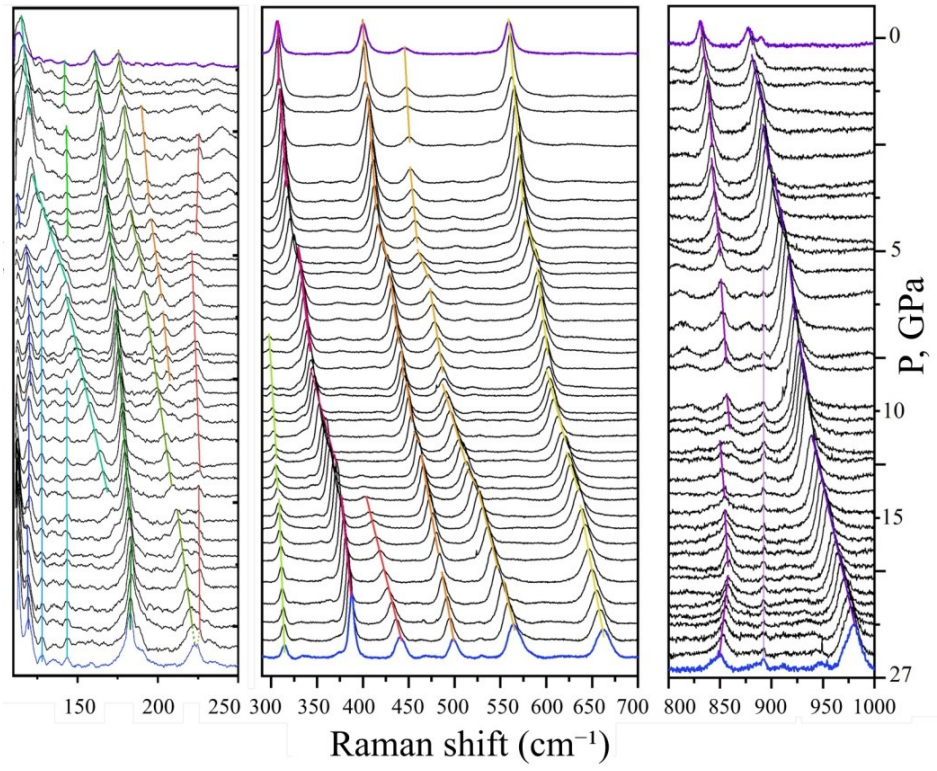

Fig. 3. Unpolarized Raman spectra of synthesized $NaGaGe_2O_6$ crystals at pressures from 0.11 to 26.08 GPa.

Acknowledgements

This study is fulfilled under Research program № FMUF-2022-0002 of the Korzhinskii Institute of Experimental Mineralogy *RAS*.

References:

Cameron M., Sueno S., Prewitt C.T., Papike J.J. High-temperature crystal chemistry of acmite, diopside, hedenbergite, jadeite, spodumene, and ureyite pyroxene // American Mineralogist. 1973. 58 594-618

Chen, J., Tian, W., Zhou, J., Lynch, V. M., Steinfink, H., Anthiram, A., May, A. F., Garlea, V. O., Neuefeind, J. C. & Yan, J. Crystal and Magnetic Structures and Physical Properties of a New Pyroxene $NaMnGe_2O_6$ Synthesized under High Pressure // Am. Chem. Soc. 2013. 135. 2776–2786.

Emirdag-Eanes, M. & Kolis, J. W. Hydrothermal synthesis, characterization and magnetic properties of $NaVGe_2O_6$ and $LiVGe_2O_6$ // Mater. Res. Bull. 2004. 39. 1557–1567.

Guyot F. et al. Comparison of the Raman microprobe spectra of $(Mg, Fe)_2SiO_4$ and Mg_2GeO_4 with olivine and spinel structures //Physics and Chemistry of Minerals. – 1986. – Т. 13. – С. 91-95.

Jiang Y. et al. Crystal Chemistry, High-Pressure Behavior, Water Content, and Thermal Stability of Natural Spodumene //Minerals. – 2025. – Т. 15. – №. 3. – С. 307.

Lambruschi E. et al. Raman spectroscopy of $CaM^{2+}Ge_2O_6$ (M^{2+} = Mg, Mn, Fe, Co, Ni, Zn) clinopyroxenes //Journal of Raman Spectroscopy. – 2015. – Т. 46. – №. 6. – С. 586-590.

Naumov G.B., Ryzhenko B.N., Khodakovsky I.L. Handbook of Thermodynamic Quantities // Moscow: Atomizdat, 1971. 240 p. (in Russian).

Nenert, G., Ritter, C., Isobe, M., Isnard, O., Vasiliev, A. N. & Ueda, Y. Magnetic and crystal structures of the one-dimensional ferromagnetic chain pyroxene $NaCrGe_2O_6$ // Phys. Rev. 2009. B. 80. 024402.

Redhammer, G. J., Roth, G., Topa, D. & Amthauer, G. Chromium-based clinopyroxene-type germanates $NaCrGe_2O_6$ and $LiCrGe_2O_6$ at 298 K // Acta Cryst. 2008. C64. i21–i26.

Redhammer G. J. et al. Nuclear and incommensurate magnetic structure of NaFeGe 2 O 6 between 5 K and 298 K and new data on multiferroic $NaFeSi_2O_6$ // Physics and Chemistry of Minerals. – 2011. – Т. 38. – С. 139-157.

Redhammer, G. J., Tippelt G. Pyroxene-type compounds $NaM^{3+}Ge_2O_6$, with M = Ga, Mn, Sc and In // Acta Cryst. 2014. C70. 852–857.

Sakamaki T. et al. Structure of jadeite melt at high pressures up to 4.9 GPa //Journal of Applied Physics. – 2012. – Т. 111. – №. 11.

Tribaudino M. et al. High-pressure Raman spectroscopy of $Ca(Mg,Co)Si_2O_6$ and $Ca(Mg, Co)Ge_2O_6$ clinopyroxenes //Journal of Raman Spectroscopy. – 2017. – Т. 48. – №. 11. – С. 1443-1448.

Wang A. et al. Characterization and comparison of structural and compositional features of planetary quadrilateral pyroxenes by Raman spectroscopy //American Mineralogist. – 2001. – Т. 86. – №. 7-8. – С. 790-806.

Wang Y., Song J., Gies H. The substitution of germanium for silicon in AST-type zeolite //Solid state sciences. – 2003. – Т. 5. – №. 11-12. – С. 1421-1433.